NAVAL POSTGRADUATE SCHOOL

MONTEREY, CALIFORNIA

THESIS

THE INFLUENCE OF BAKER BAY AND SAND ISLAND ON CIRCULATIONS IN THE MOUTH OF THE COLUMBIA RIVER

by

Kyle T. Baden

June 2014

Thesis Advisor:	James MacMahan
Second Reader:	Edward Thornton

Approved for public release; distribution is unlimited

THIS PAGE INTENTIONALLY LEFT BLANK

REPORT DOCUMENTATION PAGE

Form Approved OMB No. 0704-0188

1. AGENCY USE ONLY *(Leave blank)*	**2. REPORT DATE** June 2014	**3. REPORT TYPE AND DATES COVERED** Master's Thesis

4. TITLE AND SUBTITLE
THE INFLUENCE OF BAKER BAY AND SAND ISLAND ON CIRCULATIONS IN THE MOUTH OF THE COLUMBIA RIVER

5. FUNDING NUMBERS

6. AUTHOR(S) Kyle T. Baden

7. PERFORMING ORGANIZATION NAME(S) AND ADDRESS(ES)
Naval Postgraduate School
Monterey, CA 93943-5000

8. PERFORMING ORGANIZATION REPORT NUMBER

9. SPONSORING /MONITORING AGENCY NAME(S) AND ADDRESS(ES)
N/A

10. SPONSORING/MONITORING AGENCY REPORT NUMBER

11. SUPPLEMENTARY NOTES The views expressed in this thesis are those of the author and do not reflect the official policy or position of the Department of Defense or the U.S. Government. IRB protocol number ____N/A____.

12a. DISTRIBUTION / AVAILABILITY STATEMENT
Approved for public release; distribution is unlimited

12b. DISTRIBUTION CODE
A

13. ABSTRACT (maximum 200 words)

The Columbia River estuary is the scene of a collision between strong river discharge, considerable tidal magnitude and violent surface gravity waves that have claimed thousands of vessels and hundreds of lives. Lagrangian GPS measurements of position and surface velocity and Eulerian measurements of vertical velocity structure, temperature and salinity were used to study circulation patterns in the mouth of the Columbia River, paying particular attention to the influence of Baker Bay and the Sand Island pile dikes. Tidal range and river discharge are the key drivers in the dynamic lower Columbia River, and the presence of Baker Bay, a shallow sub-embayment, adds further complexity. Drifter velocities were greatest during maximum ebb flows and were greater in the South Channel, which is dominated by river discharge, than the North Channel, which is more heavily influenced by tidal oscillations. Drifters occasionally entered Baker Bay via Baker Inlet during flood flows, especially in conjunction with strong southwesterly winds. During ebb flows, some drifters were trapped in the Sand Island pile dike system and conducted clockwise circulations for 2–3 hours. Eulerian water temperature and salinity depend on many variables, including the semi-diurnal tides, neap-spring cycle, season, ocean upwelling and downwelling, river discharge and bathymetry. Baker Bay served as a source of contrasting water characteristics to the main channel, injecting pockets of warmer water adjacent to Sand Island following neap higher high tides during a period of high river discharge. Velocity profiles at Baker Bay, Baker Inlet, between the Sand Island pile dikes and in the main channel were analyzed to determine the degree of logarithmic behavior at each location. Unique velocity perturbations occurred in the vicinity of the pile dikes, including reversed (upriver) flow between the pile dikes during maximum ebb. Understanding unique flow patterns in river estuaries can be critical for littoral naval operations.

14. SUBJECT TERMS Columbia River, Baker Bay, Sand Island, estuary, drifter, CTD, ADCP, pile dike

15. NUMBER OF PAGES
93

16. PRICE CODE

17. SECURITY CLASSIFICATION OF REPORT	**18. SECURITY CLASSIFICATION OF THIS PAGE**	**19. SECURITY CLASSIFICATION OF ABSTRACT**	**20. LIMITATION OF ABSTRACT**
Unclassified	Unclassified	Unclassified	UU

NSN 7540-01-280-5500

Standard Form 298 (Rev. 2-89)
Prescribed by ANSI Std. 239-18

THIS PAGE INTENTIONALLY LEFT BLANK

Approved for public release; distribution is unlimited

THE INFLUENCE OF BAKER BAY AND SAND ISLAND ON CIRCULATIONS IN THE MOUTH OF THE COLUMBIA RIVER

Kyle T. Baden
Lieutenant Commander, United States Navy
B.S., Texas A&M University, 2001
M.S., The University of Southern Mississippi, 2010

Submitted in partial fulfillment of the
requirements for the degree of

MASTER OF SCIENCE IN METEOROLOGY AND OCEANOGRAPHY

from the

NAVAL POSTGRADUATE SCHOOL
June 2014

Author: Kyle T. Baden

Approved by: James MacMahan
Thesis Advisor

Edward Thornton
Second Reader

Peter Chu
Chair, Department of Oceanography

THIS PAGE INTENTIONALLY LEFT BLANK

ABSTRACT

The Columbia River estuary is the scene of a collision between strong river discharge, considerable tidal magnitude and violent surface gravity waves that have claimed thousands of vessels and hundreds of lives. Lagrangian GPS measurements of position and surface velocity and Eulerian measurements of vertical velocity structure, temperature and salinity were used to study circulation patterns in the mouth of the Columbia River, paying particular attention to the influence of Baker Bay and the Sand Island pile dikes. Tidal range and river discharge are the key drivers in the dynamic lower Columbia River, and the presence of Baker Bay, a shallow sub-embayment, adds further complexity. Drifter velocities were greatest during maximum ebb flows and were greater in the South Channel, which is dominated by river discharge, than the North Channel, which is more heavily influenced by tidal oscillations. Drifters occasionally entered Baker Bay via Baker Inlet during flood flows, especially in conjunction with strong southwesterly winds. During ebb flows, some drifters were trapped in the Sand Island pile dike system and conducted clockwise circulations for 2–3 hours. Eulerian water temperature and salinity depend on many variables, including the semi-diurnal tides, neap-spring cycle, season, ocean upwelling and downwelling, river discharge and bathymetry. Baker Bay served as a source of contrasting water characteristics to the main channel, injecting pockets of warmer water adjacent to Sand Island following neap higher high tides during a period of high river discharge. Velocity profiles at Baker Bay, Baker Inlet, between the Sand Island pile dikes and in the main channel were analyzed to determine the degree of logarithmic behavior at each location. Unique velocity perturbations occurred in the vicinity of the pile dikes, including reversed (upriver) flow between the pile dikes during maximum ebb. Understanding unique flow patterns in river estuaries can be critical for littoral naval operations.

THIS PAGE INTENTIONALLY LEFT BLANK

TABLE OF CONTENTS

I. INTRODUCTION....1

II. DATA AND METHODOLOGY....5
A. LAGRANGIAN SURFACE CURRENTS....6
B. VERTICAL VELOCITY STRUCTURE....10
C. SHORT-TERM WATER TEMPERATURE AND SALINITY MEASUREMENTS (YD 151–160)....12
D. LONG-TERM WATER TEMPERATURE AND SALINITY MEASUREMENTS (2013)....13

III. RESULTS....15
A. LAGRANGIAN SURFACE CURRENT ANALYSIS....15
1. Flood Drifter Deployments....15
2. Ebb Drifter Deployments....18
3. Baker Bay Drifter Deployment....24
4. Large Scale Flood-Ebb Drifter Deployment....25
B. VERTICAL VELOCITY STRUCTURE ANALYSIS....27
1. Pile Dike Influence....27
2. Vertical Structure....28
3. USGS Surface Velocities....38
C. SHORT-TERM WATER TEMPERATURE AND SALINITY ANALYSIS (YD 151–160)....39
1. Water Temperature and Salinity Inside Baker Bay....39
2. Water Temperature and Salinity in the Main River Channel....41
D. LONG-TERM WATER TEMPERATURE AND SALINITY ANALYSIS (2013)....43

IV. DISCUSSION....49

V. CONCLUSIONS AND RECOMMENDATIONS....57

APPENDIX A. GT-31 ACCURACY TESTING....61

APPENDIX B. DRIFTER DEPLOYMENT GRIDDED VELOCITY VECTOR PLOTS....65

LIST OF REFERENCES....71

INITIAL DISTRIBUTION LIST....73

THIS PAGE INTENTIONALLY LEFT BLANK

LIST OF FIGURES

Figure 1. Bathymetry of the lower Columbia River estuary (Stevens 2013, personal communication). Depth color scale plotted at bottom left. 3

Figure 2. Google Earth image with moored instrument locations. Blue circles indicate NPS sensor locations, green circles indicate USGS sensor locations and green/white/blue logos indicate SATURN sensor locations. 5

Figure 3. USGS north tripod surface velocities (blue) and NPS drifter deployment windows (red). 8

Figure 4. Astoria wind speed (black line, top panel) and direction (black line, bottom panel) with NPS drifter deployment windows (cyan) highlighted. 9

Figure 5. The drifter tracks for YD 145, where each color represents a drifter grouping that was released at the same time. 16

Figure 6. The drifter tracks for YD 146, where each color represents a drifter grouping that was released at the same time. 17

Figure 7. The drifter tracks for YD 148, where each line color represents an individual drifter. Cooler colors were released before warmer colors. 18

Figure 8. The drifter tracks for YD 149, where each line color represents an individual drifter. 19

Figure 9. Pile dikes at low tide (Gelfenbaum 2013, personal communication). 20

Figure 10. The drifter tracks for YD 149, zoomed in on Baker Inlet to show eddy detail. Each line color represents an individual drifter. 21

Figure 11. The drifter tracks for YD 152, where each line color represents an individual drifter. 22

Figure 12. The drifter tracks for YD 159, where each line color represents an individual drifter. 23

Figure 13. The drifter tracks for YD 151, where each line color represents an individual drifter. 25

Figure 14. YD 157 hourly gridded velocity vectors. Vector colors change with the number of hours since the initial drifter release. The drifters' turn to the north with the tide reversal can be seen in the 5^{th} hour (magenta) vectors in the eastern part of the plot. 26

Figure 15. YD 157 drifter tracks. Colors represent individual drifters. 27

Figure 16. A2 and B2 surface velocity time series (black line = tides, green line = A2 along-flow surface velocity, blue line = B2 along-flow surface velocity, 2013 yearday plotted along x-axis, velocity plotted along y-axis). Ebb velocities are negative, and flood velocities are positive. 28

Figure 17. A2 cross-flow (left) and along-flow (right) velocity profiles averaged over the eight-day collection period binned by average surface velocity. Surface velocity bins are identified in the upper left hand corner. Depth is plotted along the y-axis and velocity is plotted along the x-axis. Ebb velocities are negative, and flood velocities are positive. 29

Figure 18. A2 neap hourly velocity profiles (black line = tides, green line = A2 surface velocity, x-axis = hour of the day, y-axis = depth below the surface). 31
Figure 19. B2 velocity profiles averaged over the five-day collection period binned by average surface velocity. Surface velocity bins are identified in the upper left hand corner. Depth is plotted along the y-axis and velocity is plotted along the x-axis. Ebb velocities are negative, and flood velocities are positive. 32
Figure 20. B2 neap hourly velocity profiles (black line = tides, blue line = B2 surface velocity, x-axis = hour of the day, y-axis = depth below the surface). 33
Figure 21. Baker Inlet velocity profiles averaged over the 13-day collection period binned by average surface velocity. Surface velocity bins are identified in the upper left hand corner of the right panel. Depth is plotted along the y-axis and velocity is plotted along the x-axis. Ebb velocities are negative, and flood velocities are positive. 34
Figure 22. Baker Inlet westward cross-flow bias (black line = tides, red line = Baker Inlet mid-column cross-flow velocity, 2013 yearday plotted along x-axis, velocity plotted along y-axis). Westward velocities are negative, and eastward velocities are positive. 35
Figure 23. Baker Inlet neap hourly velocity profiles (black line = tides, red line = Baker Inlet surface velocity, x-axis = hour of the day, y-axis = depth below the surface). 36
Figure 24. Baker Bay velocity profiles averaged over the 10-day collection period binned by average surface velocity. Surface velocity bins are identified in the upper left hand corner of the right panel. Depth is plotted along the y-axis and velocity is plotted along the x-axis. Ebb velocities are negative, and flood velocities are positive. 37
Figure 25. Baker Bay neap hourly velocity profiles (black line = tides, cyan line = Baker Bay surface velocity, x-axis = hour of the day, y-axis = depth below the surface). 38
Figure 26. USGS tripod surface velocity time series. The green line represents the north tripod surface velocity, and the black line represents the west tripod surface velocity. Ebb velocities are negative, and flood velocities are positive. 39
Figure 27. Baker Bay short-term water temperature and salinity comparison between the NPS (top) and SATURN (middle) sensors and air temperature (bottom). Black lines = tides, x-axis = 2013 yearday, y-axis = temperature, color spectrum = salinity, red line = air temperature. 40
Figure 28. Main channel short-term water temperature and salinity comparison between the A2 (top), B2 (middle) and Sand Island (bottom) sensors. Black lines = tides, x-axis = 2013 yearday, y-axis = temperature, color spectrum = salinity. 43
Figure 29. 2013 SATURN water temperature and salinity measurements at Jetty-A (top) and Baker Bay (bottom). Black lines = tides, y-axes = temperature, x-axes = 2013 yearday, color spectrum = salinity. 45

Figure 30. 2013 SATURN high-frequency temperature trends and salinity measurements at Jetty-A (top) and Baker Bay (bottom). Black lines = tides, y-axes = temperature, x-axes = 2013 yearday, color spectrum = salinity. 45
Figure 31. 2013 SATURN Jetty-A (top) and Baker Bay (middle) water level and temperature correlations and river discharge magnitude at Bonneville Dam (bottom). Black lines = tides, green lines = water level and temperature correlations, blue dots = magnitude of river discharge. 48
Figure 32. Simplified diagram of hypothesized surface flows during high river discharge neap tide ebb conditions. The red arrow represents ocean water, the dark blue arrow represents river water, orange arrows represent brackish (mixed) water, medium blue arrows represent cooler river-influenced Baker Bay water originating from deeper areas of the bay, and lighter blue arrows represent warmer Baker Bay water originating from shallow tidal flats. Circular arrows represent clockwise eddies formed during ebb flows. 53
Figure 33. Simplified diagram of hypothesized surface flows during high river discharge neap tide flood conditions. The red arrow represents ocean water, the dark blue arrow represents river water, orange arrows represent brackish (mixed) water, medium blue arrows represent cooler river-influenced Baker Bay water originating from deeper areas of the bay, and lighter blue arrows represent warmer Baker Bay water originating from shallow tidal flats. 54
Figure 34. Simplified diagram of hypothesized surface flows during high river discharge spring tide flood conditions. The red arrow represents ocean water, the dark blue arrow represents river water, orange arrows represent brackish (mixed) water, and medium blue arrows represent cooler river-influenced Baker Bay water originating from deeper areas of the bay. 55
Figure 35. Simplified diagram of hypothesized surface flows during high river discharge spring tide ebb conditions. The red arrow represents ocean water, the dark blue arrow represents river water, and orange arrows represent brackish (mixed) water. Circular arrows represent clockwise eddies formed during ebb flows. 56
Figure 36. YD 145 gridded velocity vectors. 65
Figure 37. YD 146 gridded velocity vectors. 66
Figure 38. YD 148 gridded velocity vectors. 66
Figure 39. YD 149 north gridded ebb velocity vectors. 67
Figure 40. YD 149 south gridded ebb velocity vectors. 67
Figure 41. YD 151 gridded velocity vectors. 68
Figure 42. YD 152 ebb gridded velocity vectors. 68
Figure 43. YD 159 gridded velocity vectors. 69

THIS PAGE INTENTIONALLY LEFT BLANK

LIST OF TABLES

Table 1. Drifter deployment summary: deployment date, number of drifters released, tidal current orientation, deployment location, deployment duration and maximum velocity observed. 7

Table 2. Vertical velocity structure summary: instrument location, collection period, water column depth bin range, axis of maximum velocity, maximum velocity range and cross-flow velocity range. 11

Table 3. Short-term water temperature and salinity summary: instrument location, collection period, average sensor depth, temperature range and average, salinity range and average. 13

Table 4. Long-term water temperature and salinity summary: instrument location, collection period, average sensor depth, temperature range and average, salinity range and average. 14

Table 5. GT-31 static test (flat). 62

Table 6. GT-31 static test (metal plate). 62

Table 7. GT-31 static test (side). 63

Table 8. GT-31 kinematic test. 64

THIS PAGE INTENTIONALLY LEFT BLANK

LIST OF ACRONYMS AND ABBREVIATIONS

ADCP	acoustic Doppler current profiler
Baker Inlet	southern opening into Baker Bay between East Sand Island and West Sand Island
CTD	conductivity, temperature and depth instrument
GGA	National Marine Electronics Association (NMEA) sentence consisting of essential GPS fix data
GPS	Global Positioning System
GT-31	Genie GT-31 (handheld GPS unit) manufactured by LOCOSYS Technology, Inc.
NMEA	National Marine Electronics Association
NOAA	National Oceanic and Atmospheric Administration
NPS	Naval Postgraduate School
PDT	Pacific Daylight Time
psu	practical salinity unit
R^2	coefficient of determination (R squared)
RIVET-II	2013 research experiment in the Mouth of the Columbia River funded by the Office of Naval Research
RMC	NMEA sentence consisting of recommended minimum GPS position/velocity/time data
SATURN	Science and Technology University Research Network Collaboratory
SPOT	SPOT Satellite GPS Messenger (handheld GPS tracking unit)
USGS	United States Geological Survey
YD	yearday (ordinal or Julian day-of-year)

THIS PAGE INTENTIONALLY LEFT BLANK

ACKNOWLEDGMENTS

I would especially like to thank my thesis advisor, Dr. Jamie MacMahan, for his availability, patience, outstanding support and guidance during this process. It was an honor to have Dr. Ed Thornton as my second reader. From NPS, I'd like to thank Keith Wyckoff, Jenna Brown and LCDR Kate Woodall for their friendship and efforts during the field experiment. From USGS, I'd like to thank Dr. Guy Gelfenbaum, Andrew Stevens, Jenny White, Jackson Currie and Pete Dal Ferro for their outstanding support and for the use of the R/V *Parke Snavely* during the experiment. From the University of Miami, I'd like to thank Dr. Ad Reniers, Conor Smith and Patrick Rynne, who were instrumental in data collection efforts. Finally, I'd like to express my sincere gratitude to my family for their continued support.

THIS PAGE INTENTIONALLY LEFT BLANK

I. INTRODUCTION

The mouth of the Columbia River is a dynamic estuarine environment marked by the amalgamation of a river, an oceanic tide and surface gravity waves. The Columbia River is the second largest river in North America with an annual discharge rate of 2.3×10^{11} m^3 yr^{-1}, about 60 percent of the discharge rate of the Mississippi River (Klinkhammer et al. 1997). It accounts for 77 percent of the drainage between San Francisco Bay and the Strait of Juan de Fuca (Barnes et al. 1972). Although dams control the Columbia River, river discharge into the estuary varies from $2.5–11 \times 10^3$ m^3 s^{-1} over a typical year (Bottom et al. 2005). Maximum discharge occurs during late spring snowmelt freshets and during winter storms (Hickey et al. 1998).

The tidal pattern is mixed semi-diurnal with a maximum tidal range of approximately 3.6 m (Sherwood and Creager 1990). Tidal influence extends upriver all the way to Bonneville Dam at river mile 146, where river mile 0 is defined by the Portland District of the U. S. Army Corps of Engineers as "3 miles seaward from the point where the projection of a line passing through Cape Disappointment Lighthouse and North Head Lighthouse intersects the main ship channel," or at the historical seaward extent of the North and South Jetties. During spring tide ebb flows, strong tidal currents and significant freshwater discharge can result in surface currents in excess of 3 m s^{-1} at the narrow outlet to the ocean. The tidal prism, defined as the integrated volume between mean lower low and high waters, varies from about half to 10 times the river discharge volume (Hickey et al. 2010).

The interaction between the river and oceanic tide results in a density field within the estuary that alternates between weakly stratified (partially mixed), which occurs during low discharge periods with strong tides, and highly stratified (nearly salt wedge) (Hickey et al. 1998). According to Jay and Smith (1990), different mixing processes occurring under highly and weakly stratified conditions cause the salinity intrusion length for the Columbia River estuary to be a complicated function of river discharge and tidal range. The lower Columbia River splits into two major channels at Desdemona Sands (river mile 5): the North Channel, where most tidal exchange occurs, and the South

Channel, where river flow dominates. Most studies to date have focused on the main river channels where most of the interaction between the river and tide takes place (Jay and Smith 1990).

Adjacent sand flats and protected bays (such as Baker Bay) have been studied regarding biological and sedimentary processes but not concerning circulations (Jay and Smith 1990). Baker Bay is a shallow (2 m average depth) 8.5 km × 5 km basin accounting for roughly 21 percent of the surface area of the estuary between the mouth of the river and the Astoria-Megler Bridge. It is located on the Washington side of the Columbia River estuary between Cape Disappointment and Chinook Point (Figure 1). The bay is partially enclosed to the south by East Sand Island and West Sand Island. The town of Ilwaco, Washington, is located on the northwestern side of the bay, and the town of Chinook, Washington, is located on the eastern side. Two small rivers empty into Baker Bay: the Wallacut River northeast of Ilwaco and the Chinook River northwest of Chinook. Bay openings include Ilwaco Channel to the west, an inlet (hereinafter referred to as Baker Inlet) between East Sand Island and West Sand Island and an opening between the eastern shore of East Sand Island and Chinook Harbor.

According to a 2011 AECOM study, pile dikes were constructed in stages from 1885 to 1969 between the mouth of the Columbia River and Bonneville Dam to reduce dredging, protect dredge material, provide bank protection and stabilize shipping channels. The Sand Island pile dike system consists of four spur dikes constructed between 1930 and 1935. East Sand Island is a good example of a dredge spoils area protected by a pile dike system. Without the stabilizing effect of the Sand Island pile dikes, the river channel would migrate northward toward Baker Bay, and the surrounding morphology would be modified significantly (AECOM 2011).

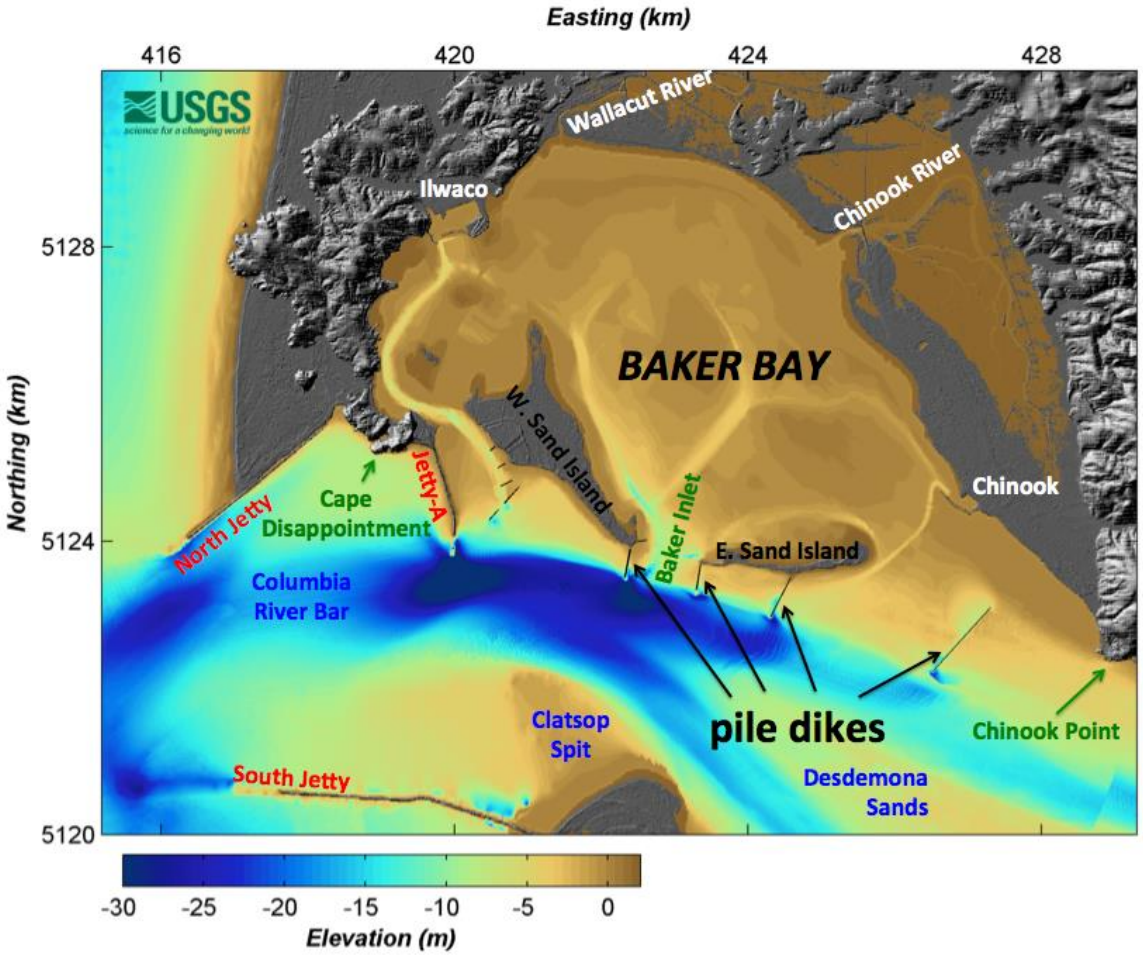

Figure 1. Bathymetry of the lower Columbia River estuary (Stevens 2013, personal communication). Depth color scale plotted at bottom left.

A large-scale research experiment (RIVET-II) was conducted in the lower Columbia River from May to June 2013. Naval Postgraduate School (NPS) data collection efforts centered on drifting buoy (drifter) deployments between the mouth of the river and the Astoria-Megler Bridge and moored surface mini-catamarans, which served as acoustic Doppler current profiler (ADCP) and conductivity, temperature and depth (CTD) instrument data collection platforms. The focus of this effort concerns the composition and circulations of water within a semi-enclosed sub-embayment (Baker Bay), interactions with barrier islands (Sand Island) and pile dikes, and the effects of these features on adjacent water masses in the lower Columbia River.

THIS PAGE INTENTIONALLY LEFT BLANK

II. DATA AND METHODOLOGY

Lagrangian surface currents, Eulerian vertical velocity structure and near-surface water temperature and salinity were the primary data collected by the NPS team. Eight multi-drifter deployments were conducted at different locations and tidal stages for estimating particle pathways and velocities. Four NPS ADCPs collected vertical velocity structure at Baker Bay, Baker Inlet, A2 and B2 (Figure 2) over a period of 4–10 days. Three NPS CTDs collected near-surface water temperature and salinity measurements at Baker Bay, A2 and B2 over a period of five to nine days. Measurements from three long-term Science and Technology University Research Network (SATURN) Collaboratory CTDs at Jetty-A, Baker Bay and Sand Island and three United States Geological Survey (USGS) tripod-mounted ADCPs in the North Channel, the South Channel and west of Jetty-A were also analyzed.

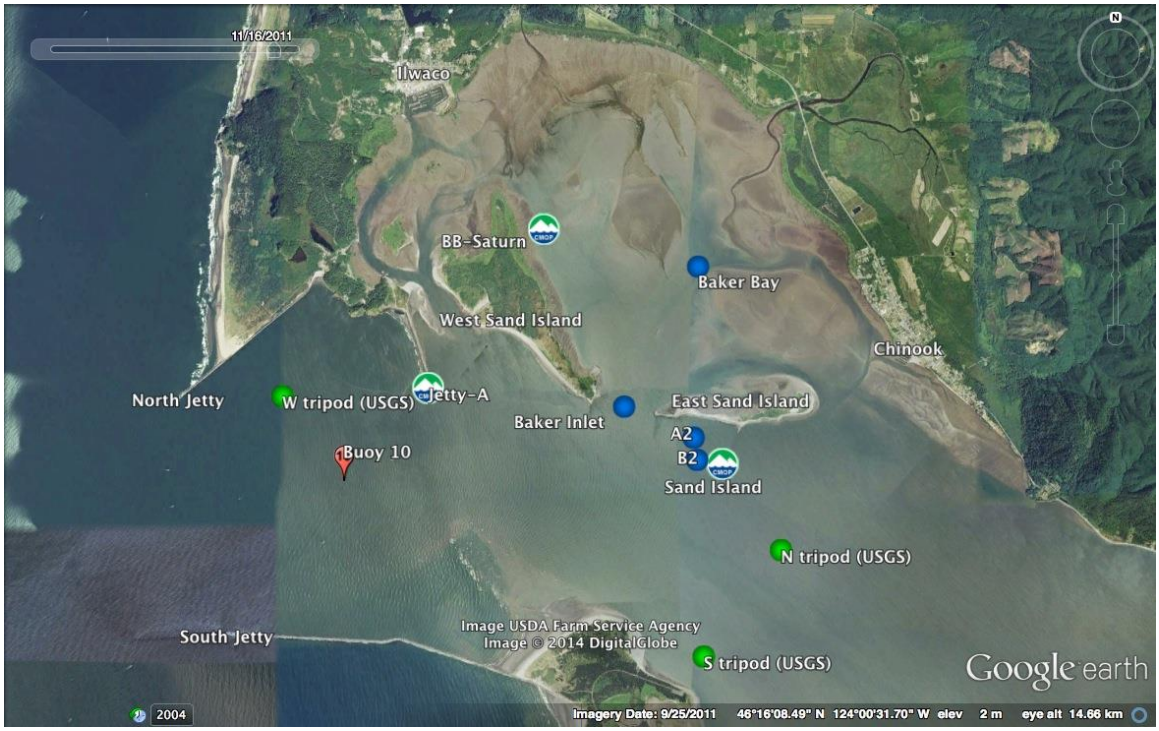

Figure 2. Google Earth image with moored instrument locations. Blue circles indicate NPS sensor locations, green circles indicate USGS sensor locations and green/white/blue logos indicate SATURN sensor locations.

A. LAGRANGIAN SURFACE CURRENTS

Lagrangian surface currents were measured using GPS-equipped drifters. Each drifter was built from a half-meter section of 20.3 cm diameter standard dimension ratio 35 polyvinyl chloride sewer pipe, capped at both ends, with four 5.7 cm holes drilled into each cap to facilitate ballasting and instrument attachment. A 2.27 kg weight was zip-tied to the bottom cap, and a foam collar was glued and zip-tied around the top cap to achieve a low center of gravity, maintaining the top of the drifter body near the waterline and reducing swaying. An orange irrigation flag was secured to each foam collar to enhance drifter visibility for daytime recovery operations while minimizing windage. A transparent, watertight OtterBox case was attached to the top cap of each drifter using Velcro and nylon straps with pinch buckles. Each case contained a 1-Hz sampling internally-logging GT-31 handheld GPS unit for high temporal resolution positioning, a 5-min sampling externally-logging SPOT handheld GPS unit for tracking drifters via satellite and a light-emitting diode cluster to facilitate nighttime recovery. GT-31 units logged time, position, Doppler speed and track angle every second. SPOT GPS trackers reported position every five minutes via satellite and could be displayed in near real-time using a Google Earth web interface. Only high-resolution GT-31 data were used in the analysis presented here. GT-31 positioning accuracy was tested under static and kinematic conditions. Analysis results are presented in Appendix A.

Eight drifter deployments were conducted between yearday (YD) 145 and 159. (Table 1). The first three deployments (YD 145, 146 and 148) were released during flood tide in the main channel near Jetty-A. The YD 149 deployment was conducted during ebb tide; drifters were nearly simultaneously released at the north and south spans of the Astoria-Megler Bridge. The YD 151 deployment was released in Baker Bay during ebb tide. The YD 152 and 159 deployments were released during ebb tide from the southern span of the Astoria-Megler Bridge. The YD 157 deployment was released in transects across the lower Columbia River during flood tide; drifters were retrieved following the subsequent ebb tide. An ebb deployment of 60 drifters was conducted on YD 155, but those data were not analyzed based on the majority of the drifters washing ashore as a result of northerly winds.

Date	# of drifters released	Ebb/Flood	Deployment location	Duration (h:mm)	Max velocity (m s^{-1})
YD 145 (5/25/13)	20	Flood	Bar	1:37	2.04
YD 146 (5/26/13)	24	Flood	Bar	2:52	1.73
YD 148 (5/28/13)	30	Flood	Bar	1:23	1.74
YD 149 (5/29/13)	30	Ebb→Flood	Astoria-Megler Bridge N&S	7:18	3.06
YD 151 (5/31/13)	40	Ebb	Baker Bay	4:58	2.28
YD152 (6/1/13)	15	Ebb→Flood	Astoria-Megler Bridge S	6:46	2.20
YD 157 (6/6/13)	84	Flood→Ebb	Bar	9:37	2.44
YD 159 (6/8/13)	20	Ebb	Astoria-Megler Bridge S	1:47	2.79

Table 1. Drifter deployment summary: deployment date, number of drifters released, tidal current orientation, deployment location, deployment duration and maximum velocity observed.

Surface velocities measured by the USGS north tripod ADCP (described in more detail later, see Figure 2 for sensor location) show spring tide conditions for the first four deployments. Maximum flood velocities decreased steadily from 1.3 m s^{-1} to 1.0 m s^{-1} between YD 145 and 149 while maximum ebb velocities alternated between −1.8 m s^{-1} following higher high water and −1.05 m s^{-1} following lower high water (Figure 3). The next three deployments (YD 151–157) were conducted during neap tide conditions; maximum flood velocities were nearly uniform around 0.8 m s^{-1}, and maximum ebb

velocities were less variable than during spring conditions (−1.4 m s^{-1} to −1.0 m s^{-1}). The final deployment (YD 159) was conducted during a transition from neap to weak spring tides.

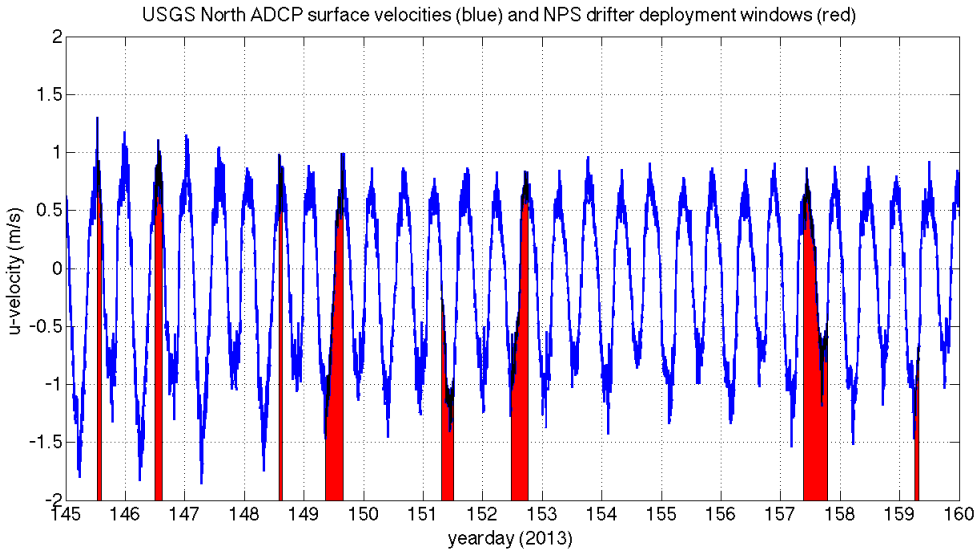

Figure 3. USGS north tripod surface velocities (blue) and NPS drifter deployment windows (red).

Wind speed and direction measurements from the National Oceanic and Atmospheric Association (NOAA) station at Astoria, Oregon (NOAA station ID 9439040), were examined to evaluate possible effects on surface currents (Figure 4). Winds were generally from the west and varied in magnitude between 0 and 8 m s^{-1}.

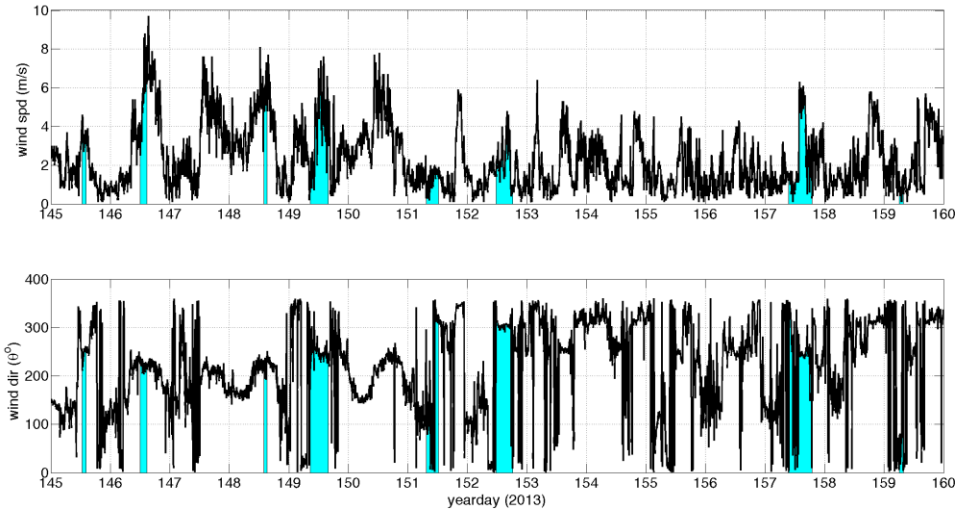

Figure 4. Astoria wind speed (black line, top panel) and direction (black line, bottom panel) with NPS drifter deployment windows (cyan) highlighted.

Statistical analysis of drifter observations was conducted using methods described by Dever et al. (1998), but instead of averaging over many tidal cycles, statistically significant average velocity fields were determined for all drifters that passed through a given grid box during a single tidal cycle during a single drifter deployment. Each deployment area was split up into 100 m grid boxes; this grid spacing criterion was chosen to provide a sufficient number of observations per grid box for high statistical confidence while maintaining sufficient resolution. Decorrelation times for each grid box were calculated based on the e-folding decay times of each velocity autocorrelation function. These values were generally 1–2 seconds, corresponding to GPS random error (i.e., noise). The number of independent observations for each grid box was calculated using

$$N = \frac{T}{t_{decorr}} = \frac{n \cdot dt}{t_{decorr}} \tag{1}$$

where t_{decorr} is the environmental decorrelation time, T is the total sampling duration, and $T = n \cdot dt$, where n is the total number of observations and dt is the instrument sampling rate (Brown et al. 2011). Plots of gridded average velocity vectors are found in Appendix B.

B. VERTICAL VELOCITY STRUCTURE

Vertical velocity structure was measured by NPS ADCPs (2 MHz Nortek Aquadopp sensors, sampling at 30-second intervals, averaged over 20 minutes) attached to moored mini-catamarans in a downward-looking orientation at four locations (Figure 2): A2 (south of East Sand Island between two pile dikes), B2 (south of A2 in the northern part of the North Channel), Baker Inlet and Baker Bay. Velocities were collected in half-meter bins from near the surface (1.7 m) to the bottom at A2, Baker Inlet and Baker Bay and one-meter bins from 2.4 m to the bottom at B2. Velocities at each location were rotated into streamwise coordinate frames using linear regression and magnetic compass declination corrections, with along-flow velocities oriented along the axis of highest velocity magnitude and cross-flow velocities oriented perpendicular to the along-flow axis (Table 2).

A2 vertical velocity structure was measured YD 152–159. A2 velocities were oriented predominantly east-west (along-river) with the axis of highest velocity about 100°/280°. Mean along-flow velocities near the surface (1.7 m) ranged between −1.12 m s^{-1} and 0.60 m s^{-1}. North-south cross-flow was very small, ranging between −0.18 m s^{-1} and 0.036 m s^{-1}.

B2 vertical velocity structure was measured from YD 152–156. B2 velocities were oriented predominantly east-west (along-river) with the axis of highest velocity about 106°/286°. Mean along-flow velocities near the surface (2.4 m) ranged between −1.31 m s^{-1} and 1.04 m s^{-1}. North-south cross-flow was very small, ranging between −0.06 m s^{-1} and 0.21 m s^{-1}.

Baker Inlet vertical velocity structure was measured YD 148–160. Baker Inlet velocities were oriented predominantly NNE-SSW, parallel to the adjacent pile dikes, with the axis of highest velocity about 027°/207°. Mean along-flow velocities near the surface (1.7 m) ranged between −1.13 m s^{-1} and 0.61 m s^{-1}. East-west cross-flow was smaller, ranging between −0.33 m s^{-1} and 0.13 m s^{-1}.

Baker Bay vertical velocity structure was measured from YD 151–160. Baker Bay velocities were oriented predominantly northeast-southwest, along a relatively deep

channel in the center of Baker Bay (Figure 1), with the axis of highest velocity about 046°/226°. Mean along-flow velocities near the surface (1.7 m) ranged between −0.48 m s^{-1} and 0.48 m s^{-1}. Cross-flow was very small, ranging between −0.04 m s^{-1} and 0.07 m s^{-1}. Maximum water depth varied between 3.7 and 6.2 m with the semi-diurnal tidal cycle.

ADCP location	Collection period	Depth range (m)	Along-flow velocity axis	Along-flow velocity range (m s^{-1})	Cross-flow velocity range (m s^{-1})
A2	YD 152–159	1.7 to 5.7	100°/280°	−1.12 to 0.60	−0.18 to 0.036
B2	YD 152–156	2.4 to 18.4	106°/286°	−1.31 to 1.04	−0.06 to 0.21
Baker Inlet	YD 148–160	1.7 to 11.2	027°/207°	−1.13 to 0.61	−0.33 to 0.13
Baker Bay	YD 151–160	1.7 to 6.2	046°/226°	−0.48 to 0.48	−0.04 to 0.07

Table 2. Vertical velocity structure summary: instrument location, collection period, water column depth bin range, axis of maximum velocity, maximum velocity range and cross-flow velocity range.

Analysis of vertical velocity structure measurements was conducted to determine the degree of logarithmic behavior at the four NPS sensor locations and to identify differences between neap and spring trends. In the logarithmic layer for rough-turbulent flow, the elevation-dependent mean current velocity, $u_c(z)$, maintains a logarithmic relationship with the elevation (z) of the form

$$u_c(z) = \frac{u_{*c}}{\kappa} \ln \frac{z}{z_0} \tag{2}$$

where u_{*c} is the shear velocity related to the mean current (u_c), κ is von Karman's constant (with a value of 0.41), and z_0 is the hydraulic roughness length (Wright 1995). The equation may be rewritten in slope intercept form ($y = mx + b$) to become

$$u_c(z) = \frac{u_{*c}}{\kappa}\left(\ln(z) - \ln(z_0)\right) \tag{3}$$

where y is $u_c(z)$, m is $\frac{u_{*c}}{\kappa}$ and x is $\left(\ln(z) - \ln(z_0)\right)$. Linear regression was used to determine the slope (m) and coefficient of determination (R^2). A more linear slope results in an R^2 value closer to one, which represents a more logarithmically shaped velocity profile. According to Lueck and Lu (1998), the height of the logarithmic layer in a tidal channel varies tidally, reaching 20 m above the bottom during peak flows of 1 m s^{-1}.

Vertical velocity structure at three USGS tripods was also analyzed to compare with NPS measurements. These tripods were located in the North Channel south of the eastern end of East Sand Island, in the South Channel east of Clatsop Spit and halfway between the North Jetty and Jetty-A (Figure 2). Velocities were collected in half-meter bins from near the bottom (8.3 m, 10.1 m and 9.2 m respectively) to the surface.

C. SHORT-TERM WATER TEMPERATURE AND SALINITY MEASUREMENTS (YD 151–160)

Near-surface water temperature and salinity were measured using NPS CTDs manufactured by Richard Brancker Research (RBR) Ltd., which sampled at 4-second intervals and were attached to mini-catamarans moored at three locations: Baker Bay, A2 and B2 (Table 3). Water temperature and salinity measurements from several SATURN sensors were analyzed to compare with NPS measurements. Air temperature measurements from the Astoria, Oregon, NOAA station were also examined to evaluate possible impacts on water temperatures.

Short-term CTD location	Collection period	Average sensor depth (m)	Temperature range and (average) (°C)	Salinity range and (average) (psu)
NPS Baker Bay	YD 151–160	0.25	13.79 to 17.89 (15.41)	1.69 to 10.09 (5.24)
SATURN Baker Bay	All of 2013	1.0	13.90 to 15.55 (15.17)	1.44 to 13.38 (6.00)
A2	YD 151–159	0.22	13.15 to 16.99 (14.73)	0 to 19.94 (5.54)
B2	YD 151–156	0.26	13.26 to 17.01 (14.59)	0.14 to 20.20 (4.69)
SATURN Sand Island	All of 2013	7.9	9.54 to 15.68 (12.99)	1.62 to 31.02 (17.13)

Table 3. Short-term water temperature and salinity summary: instrument location, collection period, average sensor depth, temperature range and average, salinity range and average.

D. LONG-TERM WATER TEMPERATURE AND SALINITY MEASUREMENTS (2013)

Long-term water temperature and salinity measurements from the SATURN stations at Jetty-A and Baker Bay (Table 4) were analyzed along with water level measurements from Hammond, Oregon (NOAA station ID 9439011), to determine relationships between the neap-spring cycle and the temperature response for 2013. All water level measurements presented in this document originated from the Hammond station. The Jetty-A sensor was located just east of the southern tip of Jetty-A at a depth of 6.4 m. The Baker Bay sensor was located approximately 2.9 km to the northeast, just east of the northern part of West Sand Island, at a depth of 1.0 m. The sampling

frequency was every 6 minutes at Jetty-A and every 15 minutes at Baker Bay. Temperature and salinity trends at Jetty-A, which represent conditions in the main river channel, were compared to measured temperature and salinity trends in Baker Bay, which are different. The influence of the neap-spring cycle at the Baker Bay station was also evaluated and helps to explain water mass circulations.

Long-term CTD location	Collection period	Average sensor depth (m)	Temperature range and (average) (°C)	Salinity range and (average) (psu)
SATURN Jetty-A	All of 2013	6.4	4.51 to 20.57 (11.29)	1.21 to 32.67 (17.13)
SATURN Baker Bay	Most of 2013 (data gaps YD 3–9, 80–113, 290–305, and 339–365)	1.0	3.62 to 20.87 (12.96)	0.79 to 25.43 (7.66)

Table 4. Long-term water temperature and salinity summary: instrument location, collection period, average sensor depth, temperature range and average, salinity range and average.

III. RESULTS

A. LAGRANGIAN SURFACE CURRENT ANALYSIS

1. Flood Drifter Deployments

On YD 145, 20 drifters were deployed in four groups beginning at peak flood tide just south of Jetty-A. Drifter groups converged initially (southeast of Jetty-A), and then diverged into three distinct groupings. Drifters released in the northernmost grouping (blue tracks in Figure 5) stayed together and moved in a straight line to the southeast for 30 minutes; then three drifters split off and traveled to the east-southeast along the North Channel (these drifters experienced higher velocities and traveled farther) while the remaining three drifters continued to the southeast. The two groups of drifters released in the center (red and green tracks in Figure 5) crossed paths about 15 minutes after deployment and combined into one group about 15 minutes later; this group followed the same path as the southeast-moving group from the northernmost release. The drifter deployed farthest south (brown track in Figure 5) moved in an arc to the northeast and passed through Baker Inlet. Tidal fronts were evident throughout the experiment and may have played a role in drifter groupings and movements. Velocities were highest during the first half of the deployment (closest to peak flood tide), and mean velocity was 1.13 m s^{-1}. Winds were light (3–4 m s^{-1}) from the west-southwest during the deployment window.

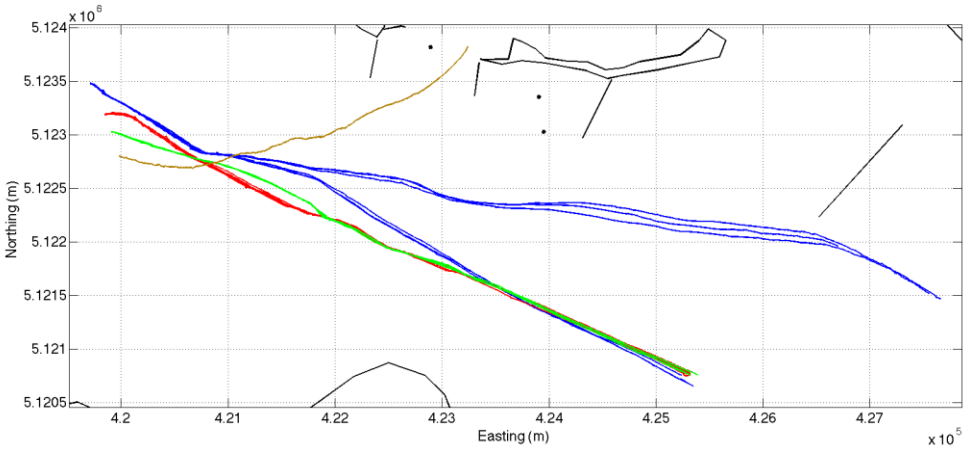

Figure 5. The drifter tracks for YD 145, where each color represents a drifter grouping that was released at the same time.

On YD 146, 24 drifters were deployed in four groups of six in a north-south transect toward Buoy 10 (see Figure 2 for location) during the start of flood tide. Flow patterns were similar to those observed on YD 145. Drifters stayed in their deployment groups for an extended period of time before dispersing. The drifters deployed in the north (blue tracks in Figure 6) diverged while passing the tip of Jetty-A and continued eastward along the North Channel. The remaining three groups of drifters converged near a common point south-southeast of Jetty-A before moving on to the east. The center groups (red and green tracks in Figure 6) traveled east, while the drifters deployed in the south (brown tracks in Figure 6) near Buoy 10 traveled an arced path to the east-northeast across the channel and then north-northeast into Baker Bay via Baker Inlet. The drifter groups were deployed at nearly the same time and were in close proximity at times but traveled along different paths. Flood velocities were highest southeast of Jetty-A, in Baker Inlet and in the North Channel. Some drifters in the blue and red groupings were slowed or deflected by pile dikes. Mean velocity was 0.75 m s^{-1}. Winds were from the southwest, increasing from 3 to 8 m s^{-1}, and likely played a role in steering drifter paths toward the Sand Island pile dikes adjacent to the North Channel.

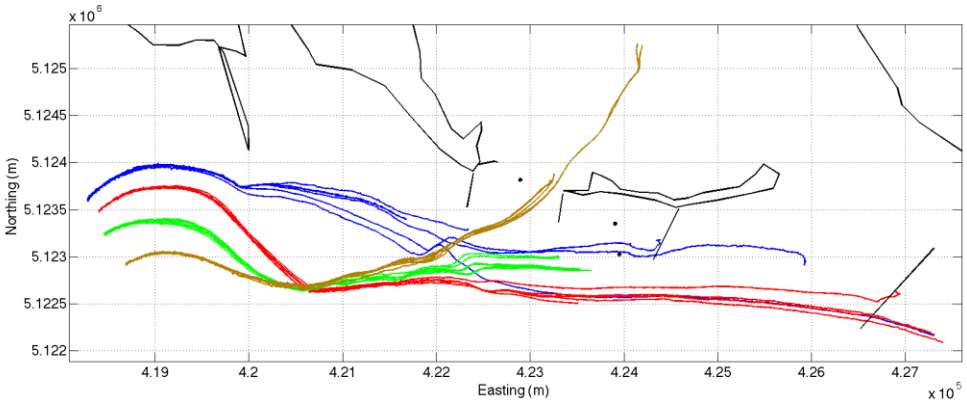

Figure 6. The drifter tracks for YD 146, where each color represents a drifter grouping that was released at the same time.

On YD 148, 30 drifters were deployed over a 12-minute period during flood tide. A south-to-north transect across the channel was planned, but a miscommunication led to the drifters being deployed along a southwest-to-northeast transect between Buoy 10 and Buoy 11 south of Jetty-A. The flow pattern was remarkably uniform, with most drifters entering Baker Bay via Baker Inlet. The drifter path into Baker Bay was likely influenced by 5–7 m s^{-1} southwesterly winds that gusted to 10 m s^{-1} during the deployed period. The seven southernmost drifters (blue tracks in Figure 7) did not enter Baker Bay, instead slowing and settling east of the pile dike along the eastern end of Baker Inlet, south of East Sand Island. The six northernmost drifters (red tracks in Figure 7) were slowed by the pile dike along the western end of Baker Inlet and entered Baker Bay more slowly than the bulk of the drifters in the center. Drifter tracks converged south of West Sand Island prior to reaching Baker Inlet, but once inside Baker Bay, drifters diverged in a fan-like pattern. Velocities were highest south of Jetty-A during the early stages of the deployment in the northernmost drifter tracks and in the center of Baker Inlet. Mean velocity was 0.82 m s^{-1}.

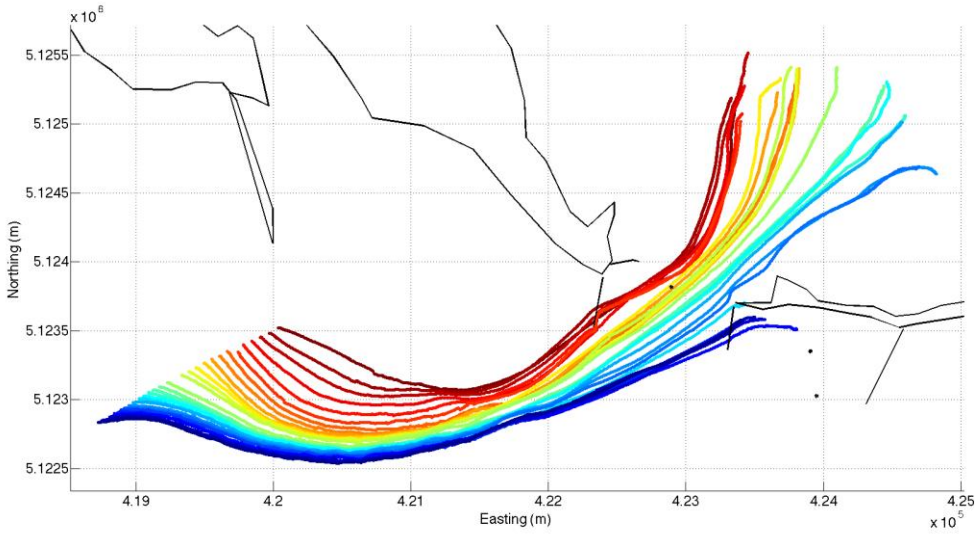

Figure 7. The drifter tracks for YD 148, where each line color represents an individual drifter. Cooler colors were released before warmer colors.

In general, flood drifters deployed in groupings tended to stay grouped (YD 145 and 146), while those released in an evenly-spaced transect tended to follow individual paths (YD 148). Drifters seemed to converge around the deep scour south of Jetty-A (Figure 1) before diverging as they approached Baker Inlet and the North/South Channel bifurcation at Desdemona Sands. Velocities tended to be highest in deeper areas south of Jetty-A and in the northern part of the main channel. Tidal fronts were observed throughout the experiment, and drifters often lined up along these water mass boundaries. Drifter tracks appeared to be influenced by winds: with lighter winds, drifter groups split up between the North Channel, the South Channel and Baker Bay; with moderate southwesterly winds, drifter tracks were biased toward the north part of the main channel, skirting the Sand Island pile dike system; and with strong southwesterly winds, almost all the drifters were pushed northeastward through Baker Inlet into Baker Bay.

2. Ebb Drifter Deployments

On YD 149, 30 drifters were deployed in two groups of 15 during ebb tide. One group was released across the northern span of the Astoria-Megler Bridge about 22 minutes prior to the release of a second group across the southern bridge span. The

southern deployment took approximately six minutes. Higher sustained velocities were experienced by the drifters in the South Channel, and most exited the mouth of the river before the following flood tide. Velocities were lower and more variable in the North Channel; those drifters that traveled the farthest reversed course with the flood tide prior to reaching Jetty-A (Figure 8). The drifters released farthest south in the northern grouping moved slowest and were possibly influenced by shallower bathymetry along those tracks; these drifters reversed course prior to reaching the Sand Island pile dikes and proceeded upriver in the North Channel during the subsequent flood tide. Winds were from the west-southwest at 2.5–7.5 m s^{-1} (gusting to 9 m s^{-1}) and may have played a role in steering drifters northward later in the deployment. Maximum ebb velocities reached 3 m s^{-1}, and mean ebb velocity was 1.4 m s^{-1}.

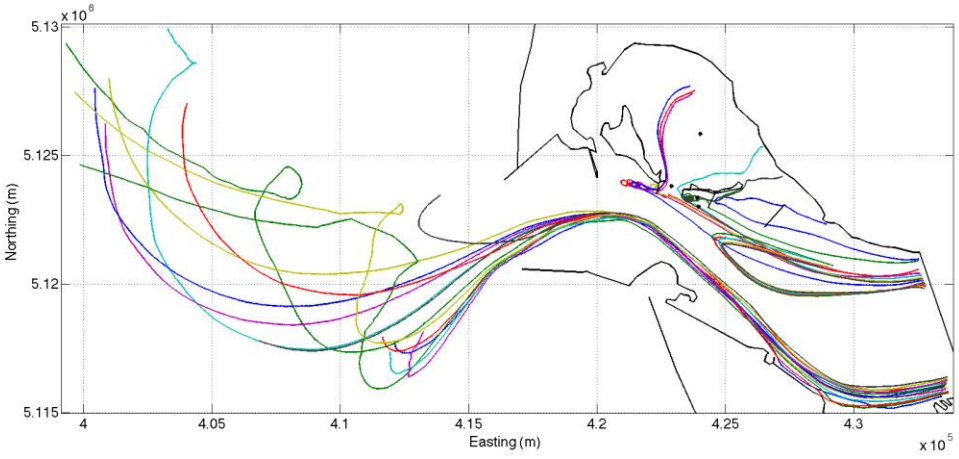

Figure 8. The drifter tracks for YD 149, where each line color represents an individual drifter.

At higher tides, the Sand Island pile dikes act as rows of porous pilings that slow down and redirect flows, but at low tides, their rock foundations become uncovered, transforming them into de facto jetties (Figure 9) that block upstream and downstream flow and facilitate eddy development in between. Some of the northern drifters stayed in

the North Channel or entered Baker Bay while others slowed in the vicinity of pile dikes and loitered in eddies south of East Sand Island or were caught in eddies south of West Sand Island (Figure 10). During ebb flows, clockwise recirculation zones developed downstream of pile dikes east and west of Baker Inlet, resembling experiments conducted by Ettema and Muste (2004) and Uijttewaal (2005). The clockwise circulations east of Baker Inlet continued for 2–3 hours (nearly half the ebb cycle) with rotation rates of 2.7–3.7 revolutions per hour depending on initial drifter speed and radii of rotation. A tidal front bordering these recirculation zones was observed along the northern edge of the main channel between Baker Inlet and Jetty-A.

Figure 9. Pile dikes at low tide (Gelfenbaum 2013, personal communication).

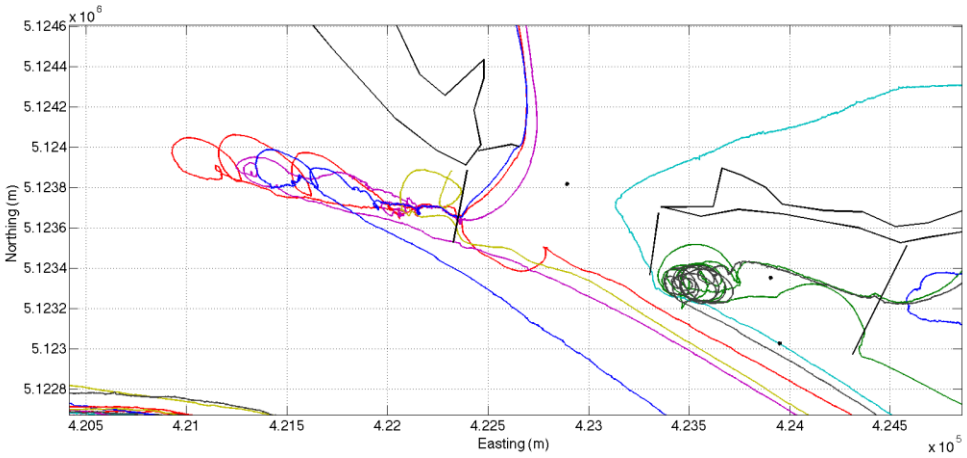

Figure 10. The drifter tracks for YD 149, zoomed in on Baker Inlet to show eddy detail. Each line color represents an individual drifter.

On YD 152, 15 drifters were released at ebb tide from the southern span of the Astoria-Megler Bridge. The last drifters were recovered during the following flood tide six hours later. Eleven GT-31s were recovered for analysis. The drifter flow pattern was relatively uniform during the ebb along the South Channel (Figure 11), but drifter paths diverged dramatically during the subsequent flood. One drifter skirted Hammond Marina, slowed down, and loitered in the vicinity of Fort Stevens. Two other drifters slowed later, near the east side of Clatsop Spit, and settled in Jetty Lagoon. One reversed course as the tide shifted to flood and entered Baker Bay via Baker Inlet. Three reversed course west of Clatsop Spit, and three reversed course downriver of Jetty-A. One drifter made it all the way out the mouth of the river. Velocities were highest during ebb tide, especially along the southern part of the main channel between Hammond and Clatsop Spit. Maximum ebb velocities reached 2.20 m s^{-1}, and mean ebb velocity was 1.18 m s^{-1}. Winds were relatively weak (1.5–4.5 m s^{-1}) from the north-northwest.

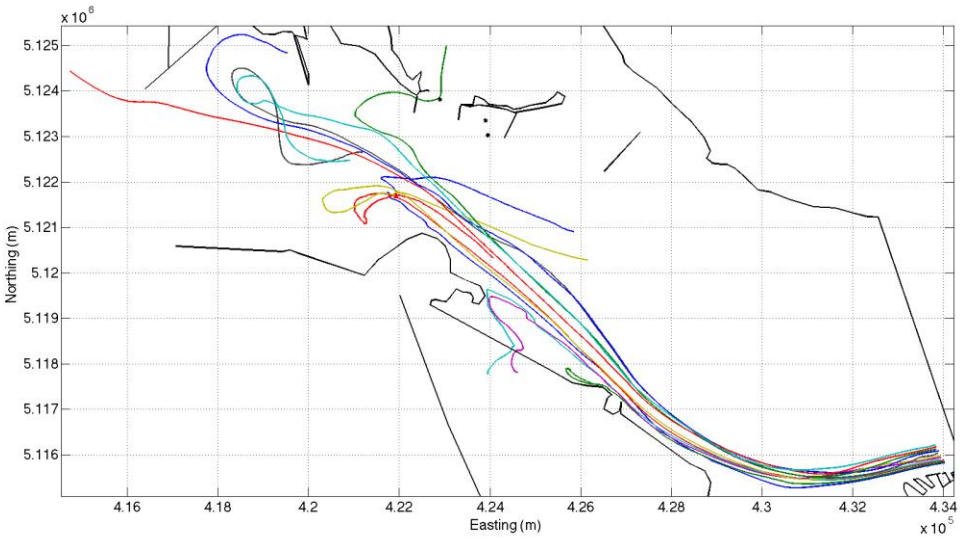

Figure 11. The drifter tracks for YD 152, where each line color represents an individual drifter.

On YD 159, 20 drifters were deployed from the southern span of the Astoria-Megler Bridge during ebb tide. The flow of drifters downriver was very uniform, and dispersion was low (Figure 12). Similar to the YD 152 ebb deployment, one drifter was slowed near Hammond Marina, and one reversed course at the eastern end of Clatsop Spit. Velocities were uniformly high between the bridge and Clatsop Spit before decreasing, as ebb flow decreased, in the vicinity of the recovery point north of Clatsop Spit. Maximum gridded velocities were 2.79 m s^{-1}, and mean gridded velocity was 2.04 m s^{-1}. Winds were northerly and weak (~1 m s^{-1}).

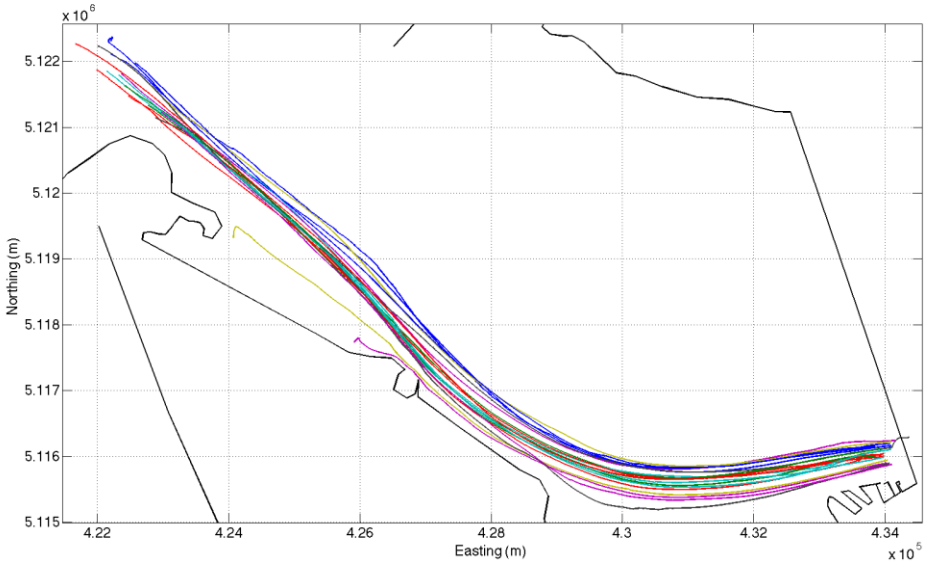

Figure 12. The drifter tracks for YD 159, where each line color represents an individual drifter.

In general, most ebb drifters exhibited smooth, almost laminar flow paths along the main river channels, especially along the South Channel. Drifters that did not flow smoothly downriver were impeded by coastal features, bathymetry or pile dikes. Winds did not appear to have as great an effect on ebb drifters as flood drifters; the combination of tidal outflow and river discharge made velocities higher and particle pathways more resistant to steering by winds. However, with southwesterly winds, some drifters were caught between pile dikes north of the main channel, others turned north with the flood tide, and still others entered Baker Bay. With northerly winds, some drifters were caught along the Oregon coast west of Astoria. The YD 149 and 159 southern bridge span releases occurred earlier in the ebb period; those drifters flowed smoothly down the South Channel and around Clatsop Spit toward the river mouth. The YD 152 deployment was released later in the ebb period, so by the time the drifters passed Clatsop Spit, the tide had reversed, and drifters dispersed in very different directions. Similar to flood deployments, velocities tended to be highest in deep areas along the main channels.

3. Baker Bay Drifter Deployment

On YD 151, 40 drifters were deployed across the northern (shoreward) perimeter of Baker Bay just after high water slack tide and were allowed to drift through the maximum ebb period. Drifter tracks were overwhelmingly westward-biased with the outgoing tide (Figure 13). As water level dropped in the bay, each drifter found its path of least resistance toward the main river channel. Most drifters released east of West Sand Island funneled toward the deeper channel running parallel to the northeastern coast of West Sand Island and then headed southeast toward Baker Inlet. Eight drifters released north and west of West Sand Island traveled westward and then southward via Ilwaco Channel or parallel to Ilwaco Channel via an adjacent tributary. Velocities were low inside Baker Bay but higher in the southern part of Ilwaco Channel and through Baker Inlet due to increasing ebb flow and deeper water depths. Highest velocities occurred during maximum ebb in the main channel just south of West Sand Island. Near the end of the deployed period, eddies formed between the pile dike extending from the western side of Baker Inlet and Jetty-A and were bounded to the south by a visually-observed tidal front. Maximum velocities reached 2.28 m s^{-1}, and mean velocity was 0.47 m s^{-1}. Winds were weak (0–2 m s^{-1}) from the northwest.

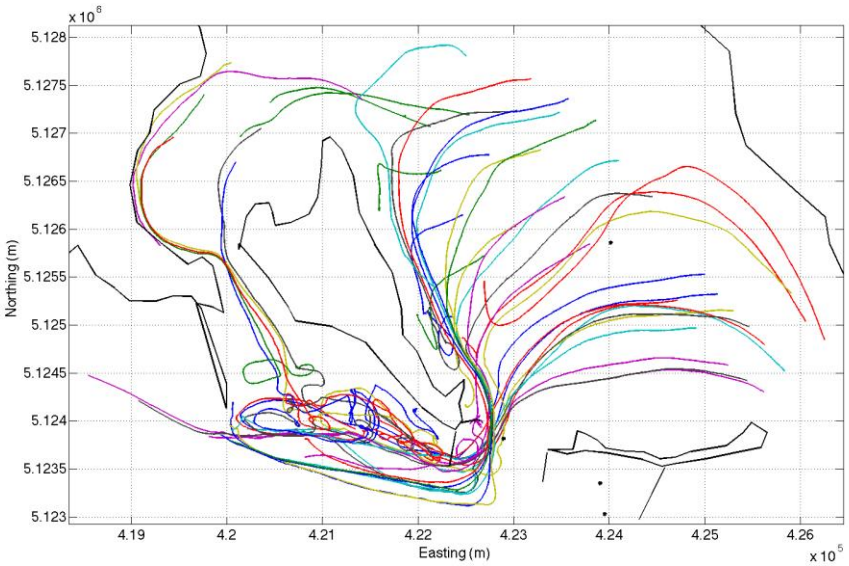

Figure 13. The drifter tracks for YD 151, where each line color represents an individual drifter.

4. Large Scale Flood-Ebb Drifter Deployment

On YD 157, 84 drifters were released in nine transects, between the North and South Jetties to the west and Baker Inlet and Clatsop Spit to the east, over a period of 87 minutes (0845L–1012L) during flood tide. Initially, velocities were low due to 0.3 m s^{-1} flood conditions and drifters loitered, so the fifth and sixth transects were postponed 10 minutes each to await stronger flood currents. Peak flood tide occurred around 1030L, and all drifters proceeded upriver across the entire channel. The farthest upriver incursion occurred in the North Channel about 1.5 km west of the northern span of the Astoria-Megler Bridge. Most drifters turned to the north during tide reversal (Figure 14), which coincided with a shift from weak northerly winds to winds of 6 m s^{-1} from the west-southwest at about 1400L (4.5 hours after the initial release). These southwesterly winds may have played a role in steering drifter paths northward during the transition to ebb tide. Maximum flood velocities reached 1.54 m s^{-1}, and mean flood velocity was 0.58 m s^{-1}. During ebb flow, those drifters that were not recovered prior to crossing the bar exited the river mouth and dispersed offshore (Figure 15), with five heading south and one heading north, eventually beaching well north of the city of Long Beach,

Washington. Some drifters were caught in eddies between West Sand Island and Jetty-A while others were caught between the pile dikes east of Baker Inlet. No drifters went into Baker Bay since the initial recovery occurred prior to the subsequent flood tide. Drifters in the South Channel tended to stay more closely grouped than those in the North Channel on their way downriver. The highest ebb velocities occurred in the bar area (Figure 1) bounded by the North Jetty, South Jetty and Jetty-A. Maximum ebb velocities reached 2.44 m s^{-1}, and mean ebb velocity was 0.58 m s^{-1}.

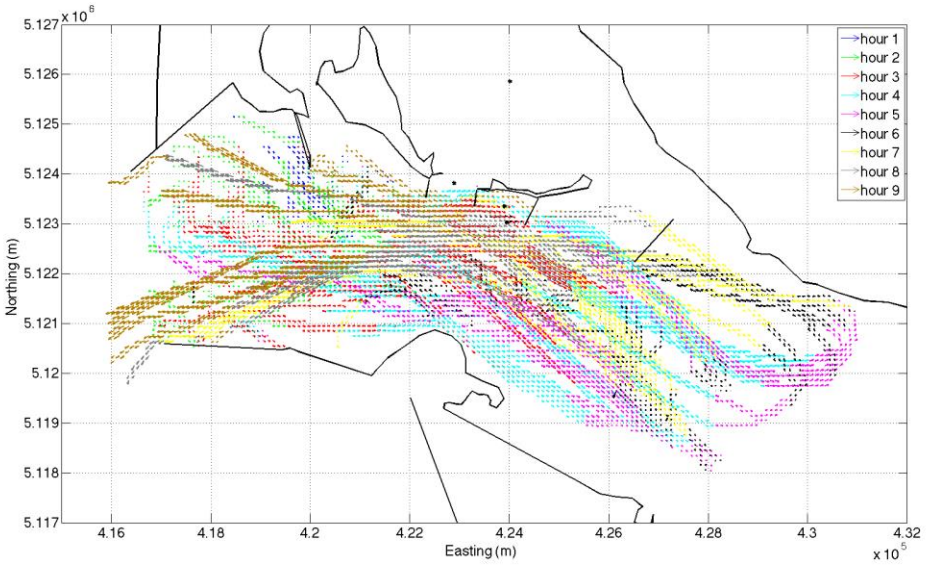

Figure 14. YD 157 hourly gridded velocity vectors. Vector colors change with the number of hours since the initial drifter release. The drifters' turn to the north with the tide reversal can be seen in the 5th hour (magenta) vectors in the eastern part of the plot.

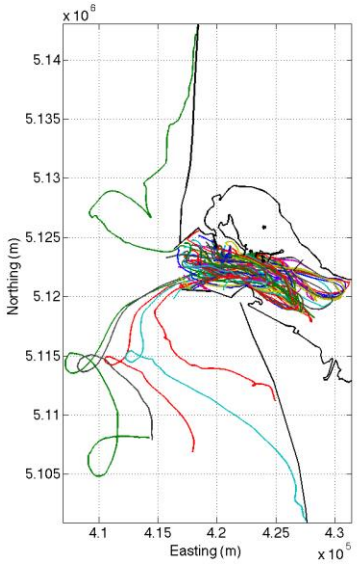

Figure 15. YD 157 drifter tracks. Colors represent individual drifters.

B. VERTICAL VELOCITY STRUCTURE ANALYSIS

1. Pile Dike Influence

The East Sand Island pile dikes had a major impact on measured surface velocities at A2 and B2 (Figure 16). At A2, flows rapidly decelerated and reversed as tidal conditions approached maximum ebb; velocities returned to zero at the low water slack. These flow reversals occurred concurrently with the formation of clockwise circulations between the pile dikes, nearest the pile dike bounding Baker Inlet, as observed in two drifter tracks from the North Channel ebb drifter deployment of YD 149 (Figure 10). Significant, repeated slowing events were observed at B2 around the same times as the ebb flow reversals at A2. Two distinct slowing events were usually observed during each maximum ebb, lasting approximately 1.5 hours each time. These slowing events produced conspicuous "fingers" in the surface velocity time series for the B2 sensor, which was located just beyond the offshore extent of the pile dikes (Figure 16). Flood and early ebb characteristics were similar at A2 and B2, although B2 flood velocity magnitudes were greater due to closer proximity to the river thalweg, the line defining the deepest channel and therefore the strongest flow.

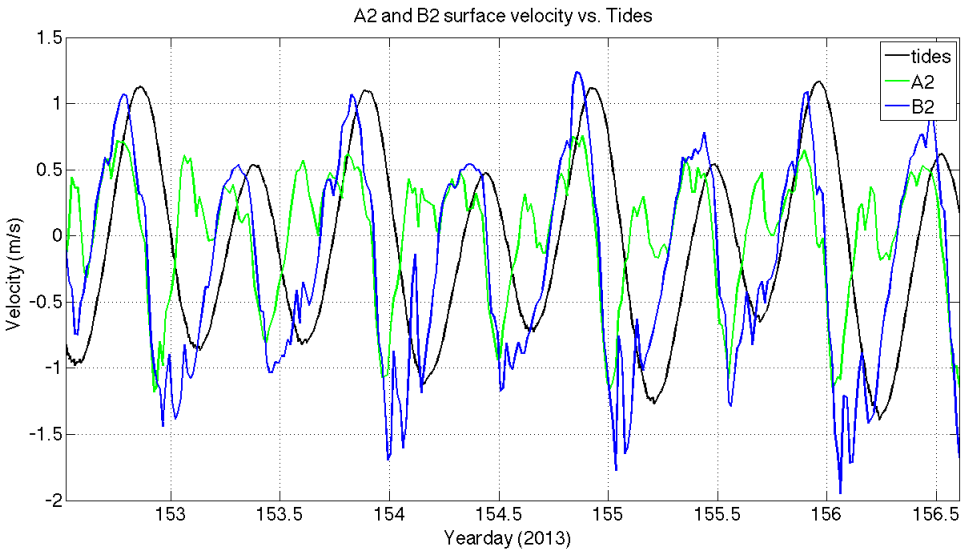

Figure 16. A2 and B2 surface velocity time series (black line = tides, green line = A2 along-flow surface velocity, blue line = B2 along-flow surface velocity, 2013 yearday plotted along x-axis, velocity plotted along y-axis). Ebb velocities are negative, and flood velocities are positive.

2. Vertical Structure

Aspects of the vertical structure of the velocity are discussed to provide the surface observations in context with the three-dimensional flow structure. The A2 streamwise velocity profiles were the most logarithmic (i.e., velocities increasing with the log of height above the bed) of the four sensors due to the sensor location being in relatively shallow water. It is believed that the depth-dependent flow effects of the pile dikes associated with changes in tidal elevation may play a role in enhancing the logarithmic response. The law of the wall R^2 values for A2 were as follows: R^2>0.5 84 percent of the time, R^2>0.75 72 percent of the time and R^2>0.9 53 percent of the time.

Time-averaged velocity profiles over the entire multi-day deployment were constructed to describe the characteristic velocity structures for the along-flow and cross-flow directions. The 20-minute average surface velocity was binned into increments of 0.25 m s^{-1} for A2, B2 and Baker Inlet and 0.1 m s^{-1} for Baker Bay. The profiles were then averaged over the experiment, and the result represents the characteristic profile for that tidal stage. However, some aspects of the profile characteristic are averaged out,

resulting in a misrepresentation, because the surface velocity can be the same for transitions between ebbing and flooding. Overall, this provides a reasonable description of the profile, but caution is required when interpreting A2 and Baker Bay time-averaged velocity profiles. For example, at A2, velocities reverse direction during ebb flows, representing a flood condition. At Baker Bay, depth is very shallow and changes dramatically with the tides, leaving deeper depth bin velocities biased toward the particular tidal stages that allow those depth bins to exist. For example, weak ebb surface velocities after higher high water were accompanied by flood velocities at depth (4–6 m) on average, while weak ebb surface velocities before lower low water occurred at very shallow water depths and had no accompanying velocity measurements deeper than 3.7 m. During these times, the temporal record is also provided to avoid bias.

At A2, ebb flows were stronger than flood flows (Figure 17). The downriver bias in upper-layer velocities, observed at other sensors, was smaller at A2 due to the velocity-mitigating effects of the Sand Island pile dikes. Binned velocity profiles exhibited a nearly true logarithmic shape, and cross-flow was minimal but slightly northward-biased.

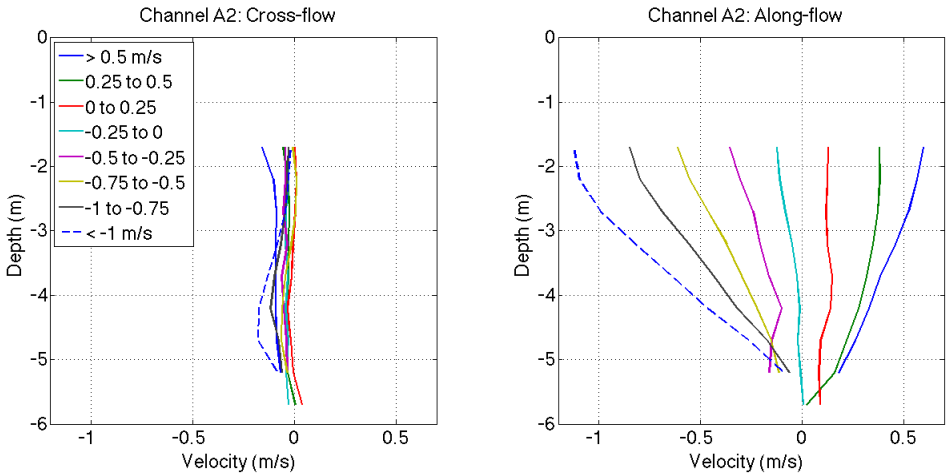

Figure 17. A2 cross-flow (left) and along-flow (right) velocity profiles averaged over the eight-day collection period binned by average surface velocity. Surface velocity bins are identified in the upper left hand corner. Depth is plotted along the y-axis and velocity is plotted along the x-axis. Ebb velocities are negative, and flood velocities are positive.

The shapes of the hourly velocity profiles were similar for neap and spring days at all stations except A2, where the ebb flow reversal caused by the pile dikes was stronger during neap tide, resulting in higher upriver velocities during maximum ebb flow (Figure 18). Individual hourly velocity profiles closely approximated a true logarithmic structure. Analysis of the evolution of hourly along-flow velocity profiles at A2 during a neap tide day (YD 153) initially reveals logarithmic downriver flow during the early ebb between higher high and lower low water. During maximum ebb flow, velocities slowed rapidly and reversed, transitioning to maximum logarithmic upriver flow in less than an hour. As the ebb weakened, logarithmic upriver flow weakened. After the lower low water slack, near zero flow persisted for one hour. During the flood between lower low and lower high water, logarithmic upriver flow developed initially before becoming non-logarithmic with a downriver bias near the surface. Just prior to lower high water, flow transitioned to logarithmic downriver flow, with maximum logarithmic downriver flow occurring one hour after lower high water. Weakening logarithmic downriver flow continued until the maximum ebb between lower high and higher low water, when once again flow reversed and transitioned to maximum logarithmic upriver flow. Logarithmic upriver flow weakened until reaching zero flow about 1.5 hours after higher low water. Logarithmic upriver flow then resumed during the remaining flood tide, attaining a slight downriver bias at the surface during maximum flood. Logarithmic upriver flow continued until higher high water, when flow reversed, becoming logarithmic downriver flow and reaching maximum downriver velocity 1.5 hours after higher high water.

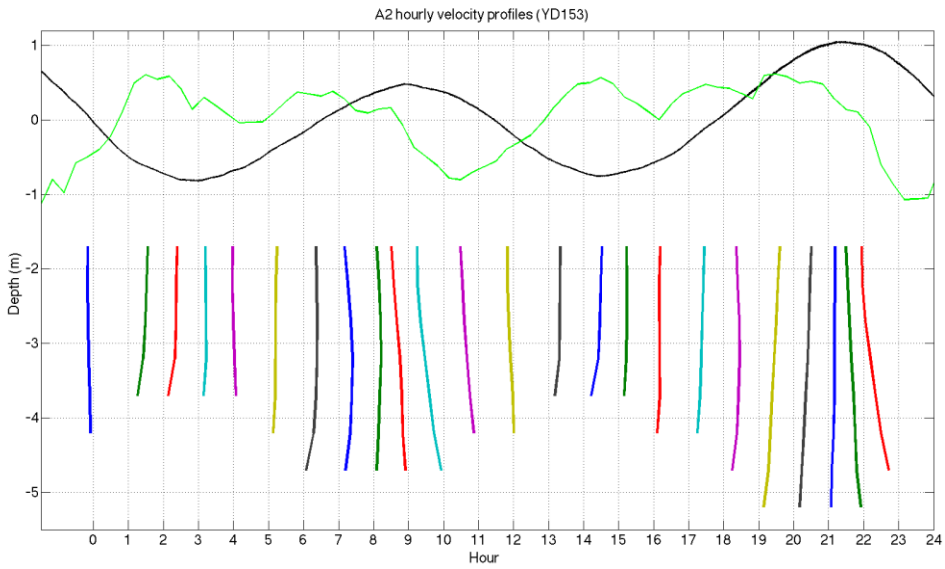

Figure 18. A2 neap hourly velocity profiles (black line = tides, green line = A2 surface velocity, x-axis = hour of the day, y-axis = depth below the surface).

The pattern of velocity profiles at B2 was the least logarithmic owing to the sensor location in the North Channel, where the tidally-driven salt wedge induces two-layer flow. The law of the wall R^2 values for B2 were as follows: R^2>0.5 53 percent of the time, R^2>0.75 17 percent of the time and R^2>0.9 2 percent of the time. The behavior at B2 is different than A2, suggesting that the salt-water wedge is restricted to the channel, and the flow between pile dikes is more closely related to one-layer response.

B2 exhibited the greatest downriver velocity bias in the upper layer (Figure 19) due to the direct influence of strong river discharge at that location. Maximum upstream velocity occurred below the surface (6.4 m), likely due to the downstream momentum of the lower density river water at the surface. During stronger ebbs (−0.75 to −1 m s^{-1}), there was a downriver velocity peak at 14.4 m. However, during moderate ebbs (−0.25 to −0.5 m s^{-1}), deep (between 12 m and 16.7 m) velocities were positive. This implies a lag in the ebb reversal, occurring first at the surface and later at depth. During flood conditions, the opposite was true: reversal occurred first at depth (ocean water) and later at the surface (river water). This implies abruptly-developing downriver flow and slowly-developing upriver flow at the surface. This could be partly due to the inequality of the

semi-diurnal tides and partly due to persistent downstream river flow. Cross-flow was minimal but slightly southward biased, opposite that observed at A2.

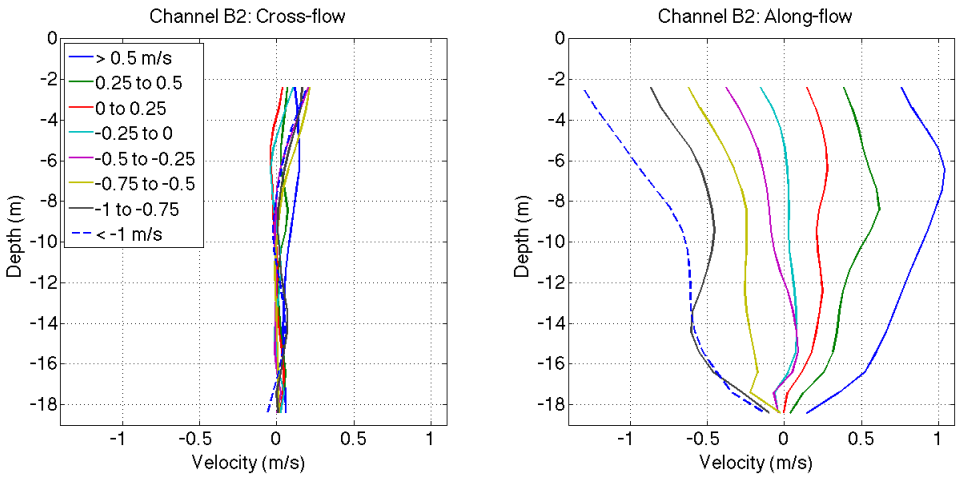

Figure 19. B2 velocity profiles averaged over the five-day collection period binned by average surface velocity. Surface velocity bins are identified in the upper left hand corner. Depth is plotted along the y-axis and velocity is plotted along the x-axis. Ebb velocities are negative, and flood velocities are positive.

Analysis of the evolution of hourly along-flow velocity profiles at B2 during a neap tide day (YD 153) initially revealed strong downriver flow at the surface, a local velocity minimum around 11 m below the surface, a local velocity maximum around 14.4 m and decreasing downriver velocity down to the bottom during the early ebb between higher high and lower low water (Figure 20). At lower low water, deep layer (12.6 m below the surface down to the bottom) flow was oriented upriver while the remaining column flow remained downriver. Two hours after lower low water, the entire column shifted to upriver flow, although the surface layer retained a relative downriver bias. At lower high water, net flow had shifted downriver (although flow around 6 m below the surface was still oriented slightly upriver). Three hours after lower high water (maximum ebb), the deep layer (14.4 m) had the strongest downriver flow. At higher low water, surface flow was downriver while deep layer (8–17 m) flow was upriver. One hour after

higher low water, the entire column exhibited upriver flow, with the highest velocity occurring mid-column; upriver flow continued until higher high water. At higher high water, there was an abrupt shift to net downriver flow with the highest velocity occurring mid-column. One hour after higher high water, flow was strongly downriver, with the highest velocity occurring at surface. A similar deep (14.4 m) downriver flow maximum occurred 1 hour after maximum ebb following lower high water on YD 153–154–155.

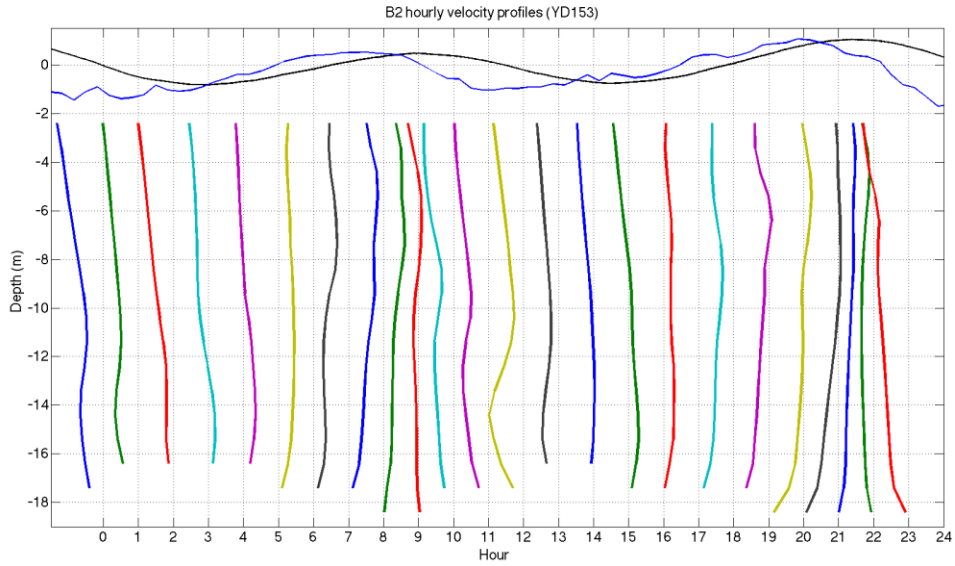

Figure 20. B2 neap hourly velocity profiles (black line = tides, blue line = B2 surface velocity, x-axis = hour of the day, y-axis = depth below the surface).

The logarithmic structure at Baker Inlet was similar to B2. Even though Baker Inlet is located between pile dikes, the flow there is parallel to the pile dikes, in and out of Baker Bay. It appears that there are different water masses that support a two-layer flow, which is not as strong as at B2. Baker Inlet represents a crossroad where warmer and mostly fresh Baker Bay water, slightly colder and fresher river water, and much colder and saltier ocean-influenced water all interact. Baker Inlet is a constricted channel exhibiting complicated flows and relatively deep depths (12 m, Figure 21). Baker Inlet R^2 values were as follows: $R^2>0.5$ 56 percent of the time, $R^2>0.75$ 34 percent of the time and $R^2>0.9$ 12 percent of the time.

Baker Inlet was characterized by strong outflow and weak inflow (Figure 21). Near the surface (1.7 m), flow was biased southward for all tidal current conditions. Maximum northward velocity occurred below the surface (3–4 m) and likely consisted of higher-density brackish water (a mixture of saltier, ocean-influenced water and fresher Baker Bay water). There was also a local north-south velocity maximum at 8–9 m depth during ebb tide.

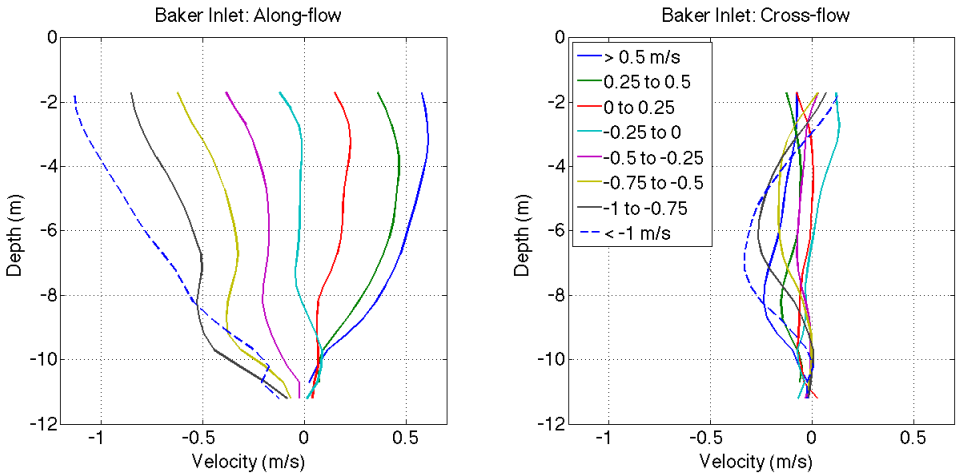

Figure 21. Baker Inlet velocity profiles averaged over the 13-day collection period binned by average surface velocity. Surface velocity bins are identified in the upper left hand corner of the right panel. Depth is plotted along the y-axis and velocity is plotted along the x-axis. Ebb velocities are negative, and flood velocities are positive.

Cross-flows were very weak at A2 and B2 (Figures 17 and 19) due to the unidirectional prevailing flows at those locations. The Baker Bay sensor's location in a relatively deep flow channel caused cross-flow to be minimal there as well (Figure 24). However, at Baker Inlet, cross-flow was significant (Figure 21). Mid-column cross-flow was biased toward the west during both ebb and flood tide and reached a maximum ebb velocity of −0.33 m s^{-1} around 7 m depth (Figure 22). Maximum eastward cross-flow occurred around 2.7 m depth during slack tide (Figure 21).

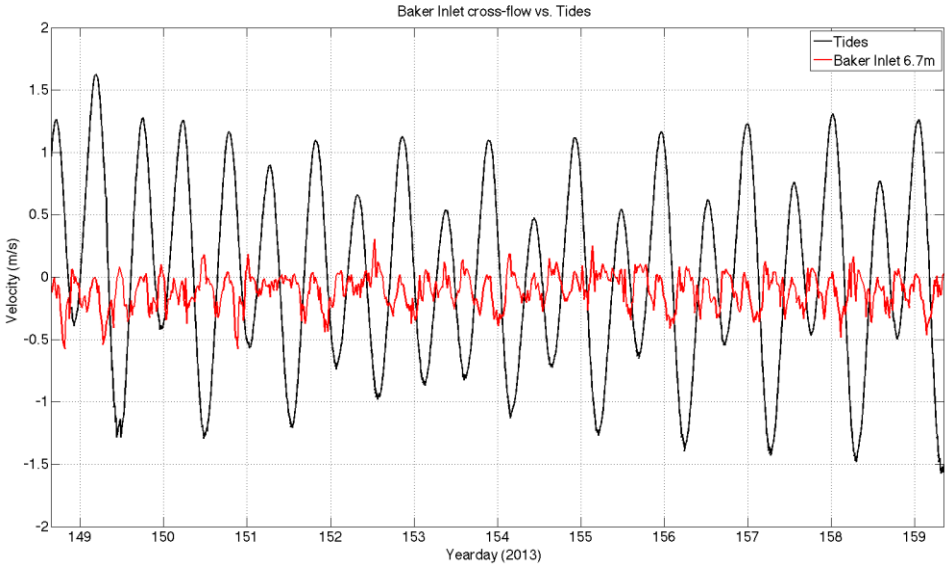

Figure 22. Baker Inlet westward cross-flow bias (black line = tides, red line = Baker Inlet mid-column cross-flow velocity, 2013 yearday plotted along x-axis, velocity plotted along y-axis). Westward velocities are negative, and eastward velocities are positive.

Baker Inlet hourly velocity profiles were less logarithmic than at A2 due to drastic transitions from inflow to outflow (Figure 23). Deep layer velocities were highest during spring tide ebb, as ocean water retreated. Analysis of the evolution of hourly along-flow velocity profiles at Baker Inlet during a neap tide day (YD 153) initially revealed downriver flow during the ebb following higher high water with the strongest downriver flow at the surface. At lower low water, deep layer (below 8 m) flow remained weakly downriver, while upper layer flow shifted to a weakly upriver orientation. Briefly logarithmic upriver flow occurred 1 hour after lower low water, and then shifted to irregular upriver flow until 1 hour prior to lower high water, when surface flow was downriver and deeper layer flow remained weakly upriver. At lower high water, net flow was downriver, continuing irregularly until higher low water; a deep layer (8.7 m) downriver flow maximum occurred during early ebb. At higher low water, surface flow orientation shifted to upriver, and deep layer flow remained weakly downriver. Ninety minutes after higher low water, the entire column flow was oriented upriver, and 3.5 hours after higher low water, the surface layer acquired a downriver bias. Just prior to

higher high water, surface layer flow had reoriented downriver, mid-layer flow was still upriver and deep layer flow was downriver. At higher high water, the entire column once again exhibited downriver flow.

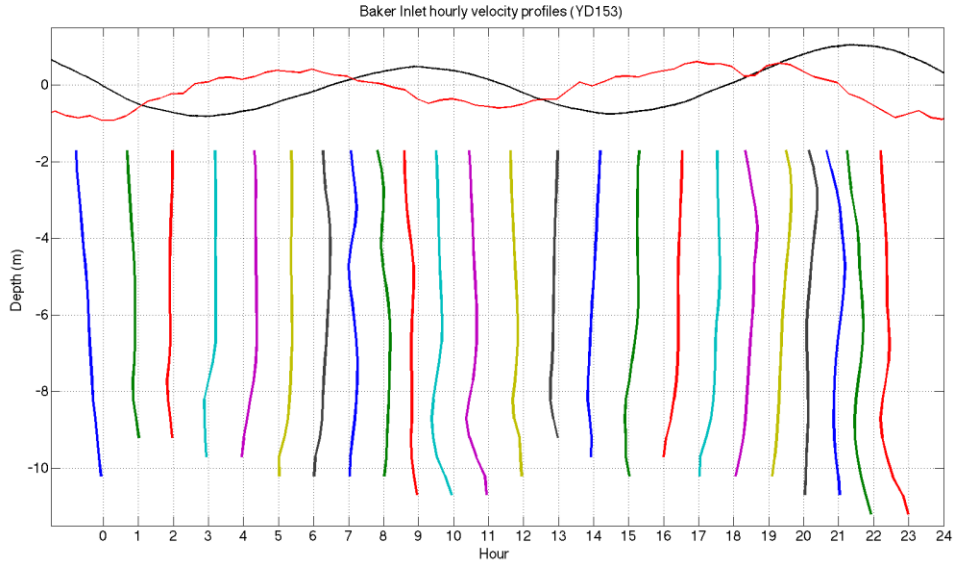

Figure 23. Baker Inlet neap hourly velocity profiles (black line = tides, red line = Baker Inlet surface velocity, x-axis = hour of the day, y-axis = depth below the surface).

Baker Bay velocity profiles were moderately logarithmic, owing to shallow water depths and relative isolation from the shoving match between strong river discharge and direct tidal surges found at Baker Inlet and B2. Baker Bay R^2 values were as follows: R^2>0.5 74 percent of the time, R^2>0.75 56 percent of the time and R^2>0.9 33 percent of the time.

Baker Bay exhibited an upper layer out-of-bay velocity bias (Figure 24) and small velocities compared to the other sensor locations. Neap and ebb flows at the surface were nearly equal in magnitude. As previously discussed, deep layer features in the average velocity profiles are misleading due to aliasing in the averaging process. Cross-flows were very small but biased southwestward near the surface.

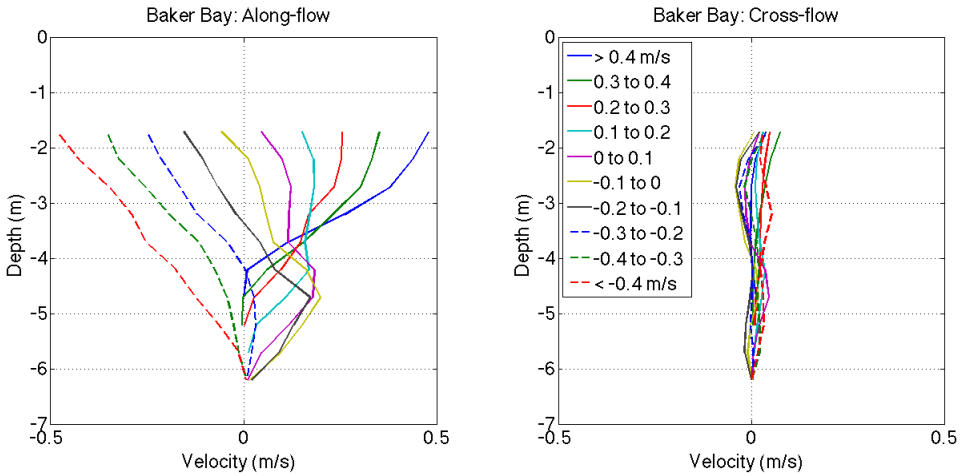

Figure 24. Baker Bay velocity profiles averaged over the 10-day collection period binned by average surface velocity. Surface velocity bins are identified in the upper left hand corner of the right panel. Depth is plotted along the y-axis and velocity is plotted along the x-axis. Ebb velocities are negative, and flood velocities are positive.

At the Baker Bay sensor, similar to Baker Inlet, deep layer velocities were highest during spring tide ebb with retreating ocean water (Figure 25). Baker Bay hourly velocity profiles were moderately logarithmic as they were shielded from the abruptly-changing velocity effects of river discharge and tides. Analysis of the evolution of hourly along-flow velocity profiles at Baker Bay during a neap tide day (YD 153) initially revealed mostly logarithmic downriver (out-of-bay) flow during maximum ebb. Column velocities near zero were measured 1 hour before lower low water. At lower low water, flow was logarithmic upriver-oriented (into-bay). One hour prior to lower high water, flow was zero near the surface and bottom with weakly upriver flow in the mid layers. At lower high water, surface to mid layer flows were oriented downriver, and mid to deep layer flows were zero. Somewhat logarithmic downriver flow existed through the weaker ebb period. One hour prior to higher low water, flow was near zero. Increasing logarithmic upriver flow occurred through the first half of the flood period. Through the second half of the flood period, the surface layer acquired a downriver flow bias. One hour prior to higher high water, surface flow was weakly downriver, and mid to deep layer flow was

weakly upriver. At higher high water, surface to mid layer flow was oriented downriver, and mid to deep layer flow was zero. After higher high water, linearly increasing downriver velocity existed from the bottom to the surface.

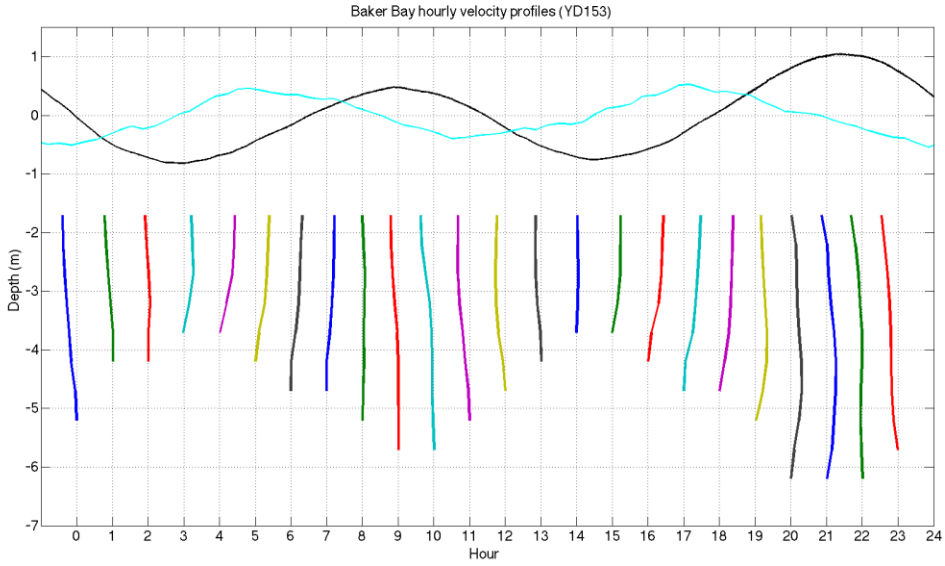

Figure 25. Baker Bay neap hourly velocity profiles (black line = tides, cyan line = Baker Bay surface velocity, x-axis = hour of the day, y-axis = depth below the surface).

3. USGS Surface Velocities

Time series of the surface velocities at the USGS tripod sensors (see Figure 2 for locations) were analyzed for comparison to NPS surface velocities. The north (green in Figure 26) and south tripod sensors exhibited expected surface velocity trends with irregular fluctuations at maximum flood and ebb. The slowing pattern observed at B2 during maximum ebb was not observed at the USGS north tripod. North velocity magnitudes were slightly higher than those in the south, possibly due to the north tripod's closer proximity to the river thalweg. However, the west (black in Figure 26) tripod surface velocities exhibited unexpected behavior. West ebb velocities were comparable to north ebb velocities, but flood velocity magnitudes were highly irregular. Very low upriver flow occurred YD 130–132, YD 135–143 and YD 152–166, while high upriver flow occurred YD 132–134 and YD 143–152. No consistent correlation between these

fluctuations and the neap-spring cycle was evident. The west tripod's location between the North Jetty and Jetty-A may have affected flow speed and direction during flood tide, and near-zero flood velocities may be indicative of shielding from the main channel upriver flow field or large-scale circulations in this zone that were evident during the YD 152 drifter deployment (Figure 11).

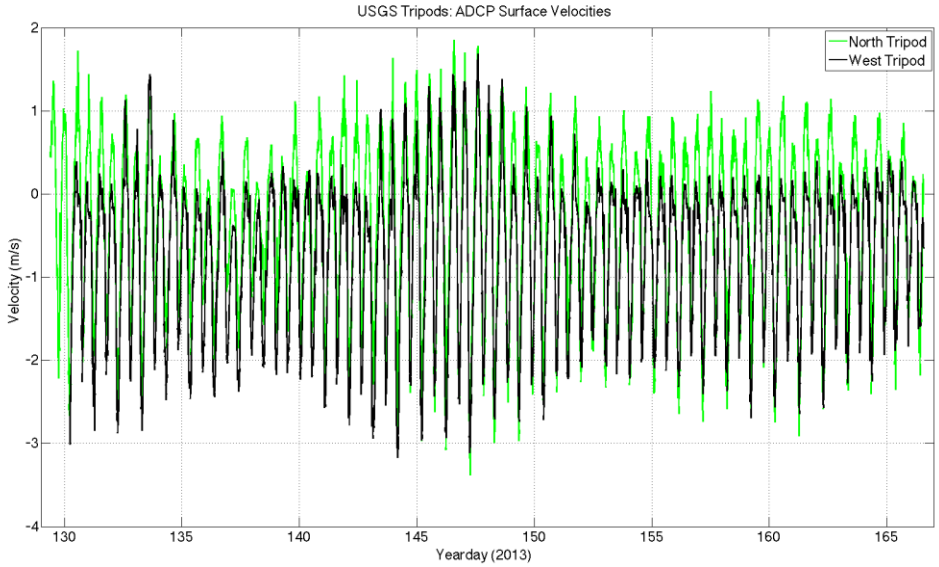

Figure 26. USGS tripod surface velocity time series. The green line represents the north tripod surface velocity, and the black line represents the west tripod surface velocity. Ebb velocities are negative, and flood velocities are positive.

C. SHORT-TERM WATER TEMPERATURE AND SALINITY ANALYSIS (YD 151–160)

1. Water Temperature and Salinity Inside Baker Bay

Water temperature and salinity measurements at the NPS Baker Bay sensor were collected as tidal conditions transitioned from neap (YD 152–156) to spring (YD 158–163). Salinity at that location and depth remained low throughout the collection period, with a range of 1.7–10.1 practical salinity units (psu) and mean of 5.2 psu (Figure 27, top). Highest salinities occurred YD 156–160 at lower low tide. During neap tide, surface temperature variation was larger, with temperatures fluctuating between 18°C at low

water and 14°C at high water, and temperature varied inversely with water level. During spring tide, surface temperature variation was smaller, and temperature varied directly with water level (opposite the neap tide scenario), with the lowest temperatures and highest salinities occurring during lower low water. This phenomenon is explored further in the Discussion chapter.

The SATURN Baker Bay sensor was located west of the NPS sensor, closer to Ilwaco Harbor, just east of the northern part of West Sand Island (Figure 2). This location and slightly deeper sensor depth resulted in marginally greater ocean influence at the SATURN sensor than the NPS sensor. Temperature increases were not as great as those observed at the NPS sensor after higher high water, and observed salinities were higher following maximum ebb than at the NPS sensor (Figure 27, middle). Highest water temperatures occurred on YD 155 at higher high water, coinciding with the highest air temperatures of the 10-day collection period (Figure 27, bottom). Differences in temperature and salinity at the SATURN and NPS Baker Bay sensors suggest different water mass characteristics and circulation patterns in different parts of the bay.

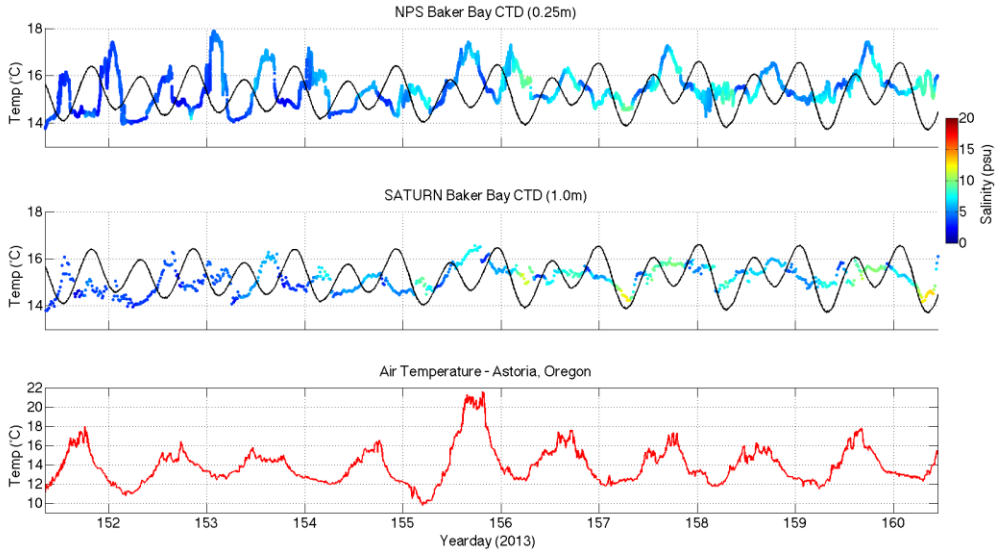

Figure 27. Baker Bay short-term water temperature and salinity comparison between the NPS (top) and SATURN (middle) sensors and air temperature (bottom). Black lines = tides, x-axis = 2013 yearday, y-axis = temperature, color spectrum = salinity, red line = air temperature.

2. Water Temperature and Salinity in the Main River Channel

Water temperature and salinity measurements for sensors A2 and B2 located outside Baker Bay are evaluated next to determine the effects of the pile dikes on water exchange. The salinity and temperature trends were very similar at A2 and B2, as seen in Figure 28 (top and middle). This may not be surprising considering the sensors are only separated by 325 m. However, each sensor exists in a different hydrodynamic regime, and based on visual observations during the experiment, a surface signature was routinely observed near the outer edge of the pile dikes suggesting that there might be a barrier that would limit exchange between the North Channel and the pile dikes. In reality, even when pile dikes blocked along-channel flow at A2 and the circulation reversed, these circulations mixed water from the North Channel into the regions between the pile dikes. Highest salinities and coldest temperatures were observed about 1.5 hours after high tide, when saltwater intrusion reached its maximum upstream extent (Figure 28, top and middle). Salinities were lower during neap tide and higher during spring tide, representing the landward extent of the ocean water, where a gradient in salinity is observed at the surface. An extended period of higher water temperatures during higher low water coincided with the warm afternoon air temperatures observed on YD 155 (Figure 27, bottom). Mean temperatures were lower during the neap part of the record (YD 151–154), consistent with the salinity behavior, as salinity-temperature trends are coupled to the different water masses.

One of the most striking features of the A2 and B2 temperature signals was dramatic 2°C temperature spikes (Figure 28, top and middle), which occurred approximately 2.5 hours after the higher high tide on YD 151–156 (neap tide). The durations of the temperature spikes were around 15 minutes. A rough calculation of surface area using an estimated ebb flow rate of 1 m s^{-1}, duration of 15 minutes and sensor separation of 325 m results in an estimated warm pocket of water ~1 km long and at least 500 m in width. The amplitudes of the temperature spikes were greater at A2 than B2. Owing to this relationship and the warmer water signal, it is believed that the source

of this water mass is Baker Bay. Interestingly, the temperature diminishes at spring tide. It is unfortunate that a longer dataset is unavailable to evaluate the long-term nature of the temperature spikes.

In contrasting Baker Bay temperature trends with those at A2 and B2, a repeated 20-hour gradual warming trend was observed between maximum ebb following higher high water and maximum flood preceding the next higher high water (Figure 28, top and middle). During neap tide, water temperature dropped sharply at maximum flood prior to higher high water, spiked 2.5 hours after higher high water and dropped again at maximum ebb. During spring tide, water temperature dropped more at lower high water than during neap tide. Similar 20-hour warming trends were observed between higher high waters during spring tide, but without the intervening temperature spikes observed during neap tide. These observations suggest that warming trends in the main river channel are governed by the influence of seawater during the semi-diurnal tidal cycle, with lowest temperatures following the farthest upriver seawater incursion at higher high water. Temperatures gradually increase during the lower low to lower high to higher low cycle before dropping once again after higher high water. Inside Baker Bay, warming and cooling trends are more dramatic and occur every 6 hours, suggesting exchange between colder main channel sources and warmer bay sources from the north.

The SATURN Sand Island water temperature and salinity measurements revealed alternating warm fresh water and cold salty water as the salt wedge moved upriver and downriver, from one side of the sensor to the other, with the tides. The sensor is located midway down the water column and measured nearly equal durations of fresh, river-influenced water and salty, ocean-influenced water. However, this deeper sensor does not measure much of the complexity observed by the A2 and B2 sensors at the surface. From YD 151 to 159, the temperature spread between fresh water and salty water increased from 1.5°C to 7°C. This change can be attributed to a combination of gradual river heating due to seasonal temperature changes and gradual ocean cooling due to enhanced offshore upwelling. The sharp salinity contrast between the two water bodies remained consistent, and stratification was strong throughout the time period of interest. During spring tide, the sensor spent more time on the salty side of the interface, so salinities were

biased toward higher values. In general, during neap tide, the smaller tidal amplitude makes the salt wedge slope more horizontal, and during spring tide, the larger tidal amplitude makes the salt wedge slope more vertical, which affects the gradient of temperature and salinity readings at the sensor.

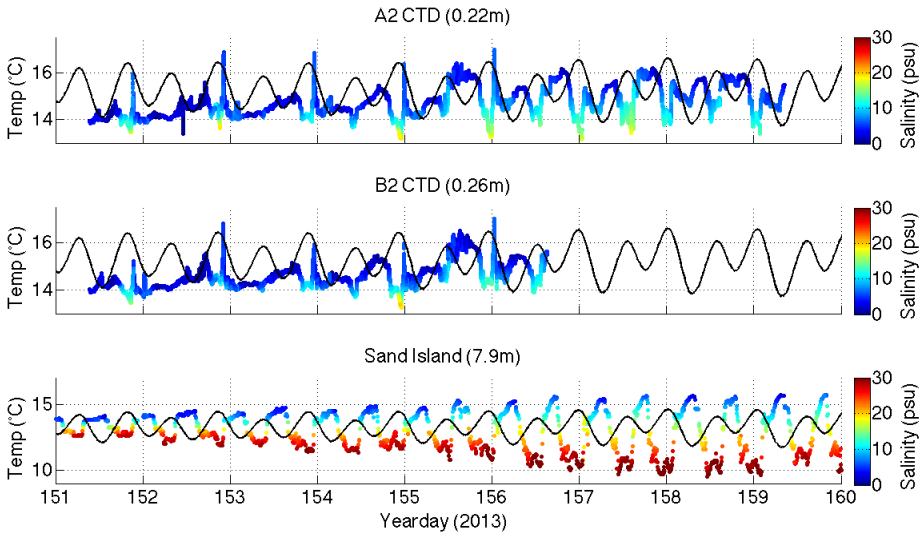

Figure 28. Main channel short-term water temperature and salinity comparison between the A2 (top), B2 (middle) and Sand Island (bottom) sensors. Black lines = tides, x-axis = 2013 yearday, y-axis = temperature, color spectrum = salinity.

D. LONG-TERM WATER TEMPERATURE AND SALINITY ANALYSIS (2013)

Long-term water temperature and salinity measurements from the SATURN stations at Jetty-A and Baker Bay are analyzed to extract more meaningful results from the relatively short-term observation period of the NPS sensors. The seasonal temperature (salinity) signal at the Jetty-A sensor has a mean of 4.5°C (17.1 psu) and range of 11.3–20.6°C (1.2–32.7 psu) (Table 4). The seasonal temperature (salinity) signal at the Baker Bay sensor has a mean of 13°C (7.7 psu) and range of 3.6–20.9°C (0.8–25.4 psu) (Table 4). The measured lower temperatures and higher salinities at Jetty-A are due to its deeper sensor depth and proximity to the ocean.

Water temperature and salinity measurements at the Jetty-A sensor reveal seasonal temperature patterns, as well as periods of ocean upwelling and downwelling. During the colder, winter months (YD 1–88 and 323–365), the ocean water was warmer than the river water, so higher salinities were observed at higher temperatures, and lower salinities were observed at lower temperatures (Figure 29, top). During warmer, summer months (YD 88–323), ocean water was colder than river water, so higher salinities were observed at lower temperatures, and lower salinities were observed at higher temperatures. Periods of greater daily temperature variation are indicative of enhanced ocean upwelling (e.g., YD 190–240, Figure 29, top), as divergence at the ocean surface drew colder ocean water upward, cooling the ocean water that entered the estuary. Periods of smaller daily temperature variation are indicative of periods of enhanced ocean downwelling (e.g., YD 133–139, 145–148 and 176–178, Figure 29, top), as convergence of warmer ocean surface water pushed warmer ocean water downward, deepening the warmer upper ocean layer and resulting in warmer ocean water entering the estuary.

The 2013 SATURN Baker Bay water temperature and salinity measurements show that Baker Bay temperature trends (Figure 29, bottom) generally followed the river-influenced part of the Jetty-A temperature and salinity plot. Salinity was relatively low overall, but brackish conditions were evident, especially during a period of lower river discharge (YD 195–261) and during spring tide cycles. YD 262–291 salinity values were suspect (anomalously low), possibly due to biofouling of the conductivity sensor.

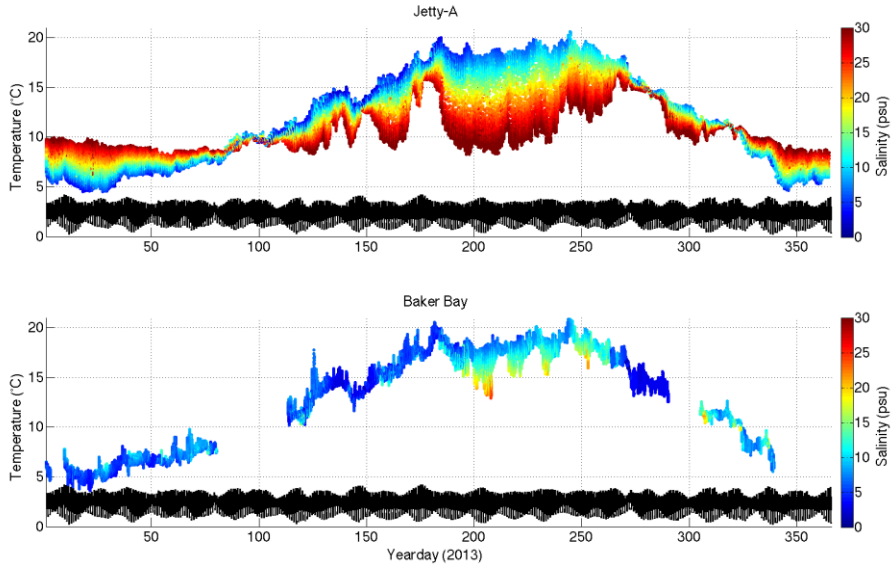

Figure 29. 2013 SATURN water temperature and salinity measurements at Jetty-A (top) and Baker Bay (bottom). Black lines = tides, y-axes = temperature, x-axes = 2013 yearday, color spectrum = salinity.

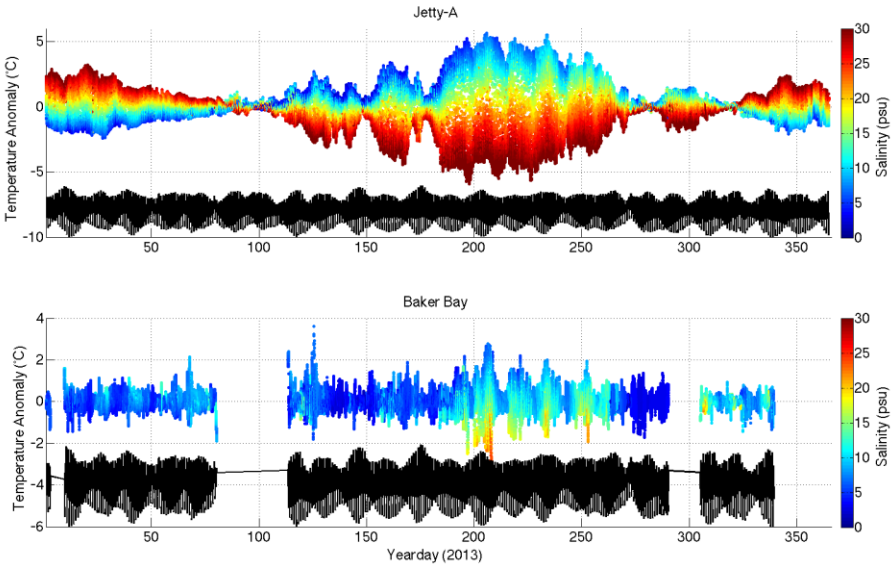

Figure 30. 2013 SATURN high-frequency temperature trends and salinity measurements at Jetty-A (top) and Baker Bay (bottom). Black lines = tides, y-axes = temperature, x-axes = 2013 yearday, color spectrum = salinity.

Temperatures were high-pass filtered to eliminate seasonal temperature trends and to focus on diurnal temperature changes due to ocean and river interplay (Figure 30). Examining a two-day running correlation between water level and high-pass temperature in Baker Bay allowed diagnosis of ocean influence in Baker Bay and how it changed seasonally and with the neap-spring cycle. First, the two-day running correlation was determined for the SATURN Jetty-A sensor (Figure 31, top), which represented conditions in the main river channel mid-way down the water column. A two-day window and 6-minute time step provided the best resolution of the neap-spring cycle's influence on correlation trends. At Jetty-A, small perturbations in the correlation were induced by the neap-spring cycle, but generally, the correlation was strongly positive (near +1) when ocean temperatures were warmer than river temperatures (YD 1–88 and 323–365, Figure 31, top). Rising tides were responsible for increasing water temperature at the Jetty-A sensor for all tidal ranges. Conversely, the correlation was strongly negative (near −1) when ocean temperatures were colder than river temperatures (YD 88–323, Figure 31, top). Rising tides resulted in decreasing water temperature at the Jetty-A sensor for all tidal ranges. The closer the ocean and river temperatures were to each other, the more "unstable" the correlation. The near-zero correlations around YD 101 and YD 281 may be explained by river and ocean temperatures being roughly equal at those times. YD 101 also marked the first peak in the magnitude of river discharge for the season (Figure 31, bottom).

The water level and temperature correlation at the SATURN Baker Bay sensor was much more complex (Figure 31, middle). In general, this correlation was opposite and smaller in magnitude than the correlation at the Jetty-A sensor. The Baker Bay correlation was generally negative when ocean water was warmer than river water and positive when ocean water was colder than river water (Figure 31, middle) during periods of weaker river discharge (YD 20–70 and YD 180–240, Figure 31, bottom). This opposite correlation illustrates a 6-hour time lag or 180° phase lag between water level changes and temperature changes in Baker Bay due to the location of the SATURN Baker Bay sensor, which is shielded by West Sand Island. Ocean-influenced water must

travel north of West Sand Island while mixing with fresh water during flood tide, and this brackish water cannot flow southward across the sensor until the following ebb tide.

During the high river discharge associated with the spring freshet period (YD 121–177), Baker Bay experienced alternating positive and negative correlations with the neap-spring cycle (Figure 31, middle). During spring tides (e.g., YD 157–163), ocean-influenced water reached the Baker Bay sensor, and the correlation was positive (Figure 31, middle), as would be expected during this warmer season. However, during neap tides (e.g., YD 150–155), the strong river discharge prevented much of the ocean-influenced water from reaching the Baker Bay sensor at all, resulting in a negative correlation (Figure 31, middle). Based on analysis of short-term neap tide water temperature and salinity trends, it is hypothesized that colder fresh water from the deeper southern part of Baker Bay is pushed northward across the sensor during flood flows, and warmer fresh water from the shallower northern Baker Bay tidal flats is pulled southward across the sensor during ebb flows, resulting in a predominantly negative correlation during high discharge neap tides. This hypothesis is further investigated in the Discussion chapter.

During times of the year when ocean water was warmer than river water (YD 1–87 and 324–365), river discharge was low (Figure 31, bottom) and neap-spring correlations at Baker Bay were not as significant (Figure 31, middle). For YD 305–339, neap-spring conditions appeared to have an effect on the water level and temperature correlation similar to that observed YD 121–177, but analysis was clouded by an apparent time lag of 3–5 days and a seasonal shift in relative water temperature around YD 323. Stretches of missing data at the SATURN Baker Bay sensor prevented a complete annual analysis (Figure 31, middle).

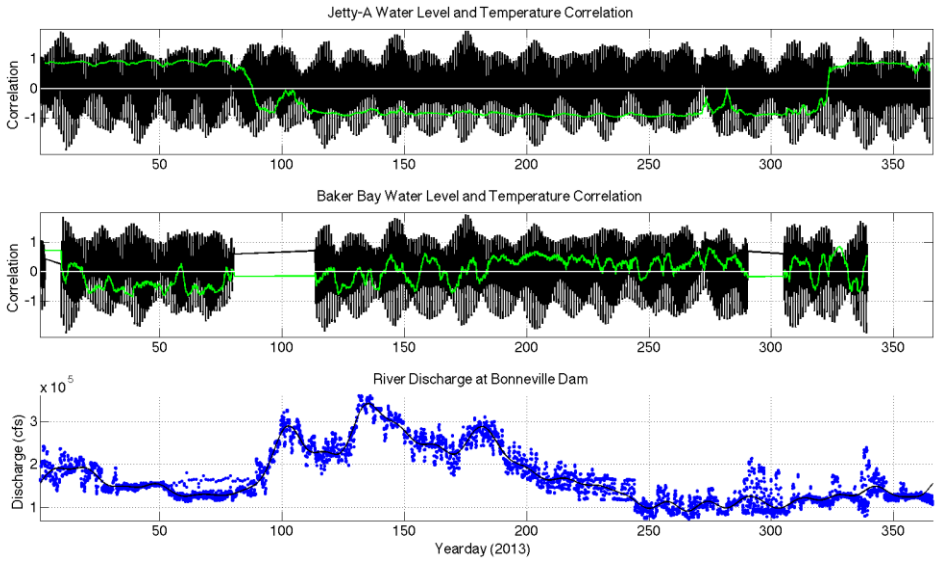

Figure 31. 2013 SATURN Jetty-A (top) and Baker Bay (middle) water level and temperature correlations and river discharge magnitude at Bonneville Dam (bottom). Black lines = tides, green lines = water level and temperature correlations, blue dots = magnitude of river discharge.

IV. DISCUSSION

Synthesizing Lagrangian surface current measurements, vertical velocity structure measurements and water temperature and salinity measurements allows an opportunity to conceptualize the surface flows in and around Baker Bay during a 10-day window (YD 151–160) spanning a neap-spring transition during the season of highest river discharge. The first part of the time period (YD 151–156) was during neap tide conditions, and the second part (YD 156–160) was during spring tide conditions. A series of simplified diagrams are provided to summarize hypothesized surface flows (Figures 32–35).

Lagrangian surface current patterns differed during flood and ebb conditions. Flood flows were generally biased toward the northern part of the main channel (Figures 5–7), where previous studies have shown that tidal influence preferentially manifests itself (Jay and Smith 1990). A closer look at the bathymetry of the North Channel shows sand waves oriented upriver (Figure 1), supporting this concept. Ebb flows were generally stronger in the southern part of the main channel, where river discharge dominates (Figure 8). Ebb flows were also generally more organized, exhibiting smooth downriver streamlines (Figures 8, 11 and 12). Drifters that came into contact with the Sand Island pile dike system were slowed and/or redirected (e.g., Figures 6, 7 and 10). Whether or not flood drifters entered Baker Bay seemed to depend on their trajectory after passing Jetty-A; the southernmost groupings tended to drift northeastward toward Baker Inlet while northern groupings tended to stay in the main channel along paths steered by the pile dike system (Figures 5 and 6). Ebb drifters released from the northern span of the Astoria-Megler Bridge did not enter Baker Bay via the eastern opening. Instead, they were redirected toward the main channel by the Sand Island pile dikes, with some entering Baker Bay via Baker Inlet during the subsequent flood tide (Figure 8). Surface winds seemed to impact surface currents and therefore drifter trajectories. This was especially evident on the flood deployment of YD 148, when almost all of the drifters were pushed through Baker Inlet into Baker Bay (Figure 7). The ebb deployment inside Baker Bay provided evidence of the flow pathways that drifters preferentially migrated toward and traveled along (Figure 13). Most drifters congregated in the deeper

channel along the northeastern coast of West Sand Island before exiting the bay via Baker Inlet while others found deeper channels northwest of West Sand Island (near Ilwaco) and exited the bay via Ilwaco Channel. The large-scale flood-ebb drifter deployment on YD 157 illustrated a wide variety of drifter tracks (Figure 15) and provided evidence suggesting that once drifters exit the mouth of the river, they are not likely to come back into the estuary.

Eulerian surface velocity measurements at B2 and A2 revealed the flow slowing and reversing effects of the Sand Island pile dikes during ebb flows (Figure 16). Eddies that developed concurrently with the flow reversals were observed during ebb drifter deployments (Figures 10 and 13). The A2 surface velocity record showed that the flow reversals occur between the Sand Island pile dikes repeatedly, with each ebb cycle (Figure 16).

Vertical velocity structures revealed the degree of logarithmic behavior of velocity profiles at each sensor. A logarithmic velocity profile is indicative of well-mixed turbulent flow in a one-layer fluid. The velocity profiles at A2 exhibited the most logarithmic structure (53 percent of the deployment with R^2>0.9, Figure 18), followed by Baker Bay (33 percent of the deployment with R^2>0.9, Figure 20), Baker Inlet (12 percent of the deployment with R^2>0.9, Figure 23) and B2 (2 percent of the deployment with R^2>0.9, Figure 25). The pile dikes bounding the A2 sensor, and the sheltered location of the Baker Bay sensor dampened some of the erratic velocity effects observed at B2 and Baker Inlet, which periodically exhibited two-layer flow. Generally, velocity orientation at the surface was consistent with the rest of the column, especially at the shallower sensor locations (i.e., A2 and Baker Bay). Time lags in flow direction changes were evident at the deeper sensor locations (i.e., B2 and Baker Inlet). Average velocity profiles exhibited expected variability with the flood-ebb cycle: velocities were upriver during flood tides and downriver during ebb tides (Figures 17, 19, 21 and 24). Ebb velocities were stronger than flood velocities due to the cumulative effect of retreating oceanic tides and outgoing river discharge. Velocities were generally highest at the surface and lowest near the bottom, owing to boundary layer frictional effects. Velocities were higher in deeper locations closer to the river thalweg; B2 measured higher velocities

than A2, and Baker Inlet measured higher velocities than Baker Bay (Table 2). Cross-flow velocities were minimal except at Baker Inlet, which exhibited westward-biased mid-column velocities (Figure 22).

Long-term water temperature and salinity measurements revealed a seasonal pattern of water temperature changes with respect to the semi-diurnal tidal cycle. At the SATURN Jetty-A sensor in the main channel, the correlation between water level and temperature was positive in colder (winter) months and negative in warmer (summer) months (Figure 31, top), reflecting the seasonal changes in differential temperature between ocean water and river water. At the SATURN Baker Bay sensor, the seasonal correlation was opposite (Figure 31, middle) owing to the indirect influence of ocean water at that sensor location; ocean-influenced water reached the Baker Bay sensor during the outgoing tide as opposed to the incoming tide. However, during a period of high river discharge (Figure 31, bottom) associated with the spring freshet (YD 121–177), the seasonal pattern was interrupted, and correlations instead alternated with the neap-spring tidal cycle (Figure 31, middle). High discharge water level and temperature correlations followed the normal seasonal trend during spring tides but were opposite during neap tides.

The short-term water temperature and salinity measurements help to clarify the complex story of neap and spring surface flows in and adjacent to Baker Bay during the collection period (YD 151–160), which occurred across a neap-spring cycle during the period of high river discharge. Simplified diagrams summarize hypothesized surface flows for a neap tide ebb period, a neap tide flood period, a spring tide flood period and a spring tide ebb period.

During neap tide ebb periods, cool fresh river water supplanted colder brackish ocean-influenced water in the main river channel adjacent to Baker Bay with the outgoing tide (Figure 32). Surprisingly, after neap tide higher high waters, temperature spikes lasting about 15 minutes were observed at A2 and B2 (Figure 28, top and middle). Because these spikes were 2°C warmer than prevailing river temperatures and occurred during ebb flows, it is hypothesized that the source of these pockets of warmer water was the warm, shallow tidal flats of Baker Bay and that the pathway to the A2 and B2 sensors

was from upriver, between East Sand Island and Chinook Harbor. Meanwhile, inside Baker Bay, warm (~18°C) fresh water from the shallow northern tidal flats was drawn southward across the two Baker Bay sensors (Figure 27, top and middle) as cooler fresh water exited the bay via Baker Inlet with the outgoing tide (Figure 32). Daytime heating may have played a minor role in water temperature trends. The most significant daytime heating occurred on YD 155, with air temperatures reaching 21.5°C (Figure 27, bottom). Water temperature at the NPS Baker Bay sensor reached 17.4°C that afternoon at higher low water and 17.3°C overnight during the subsequent maximum ebb tide (Figure 27, top). As observed during ebb drifter deployments, clockwise circulations developed between pile dikes west of the A2 sensor, south of West Sand Island and between Jetty-A and the North Jetty.

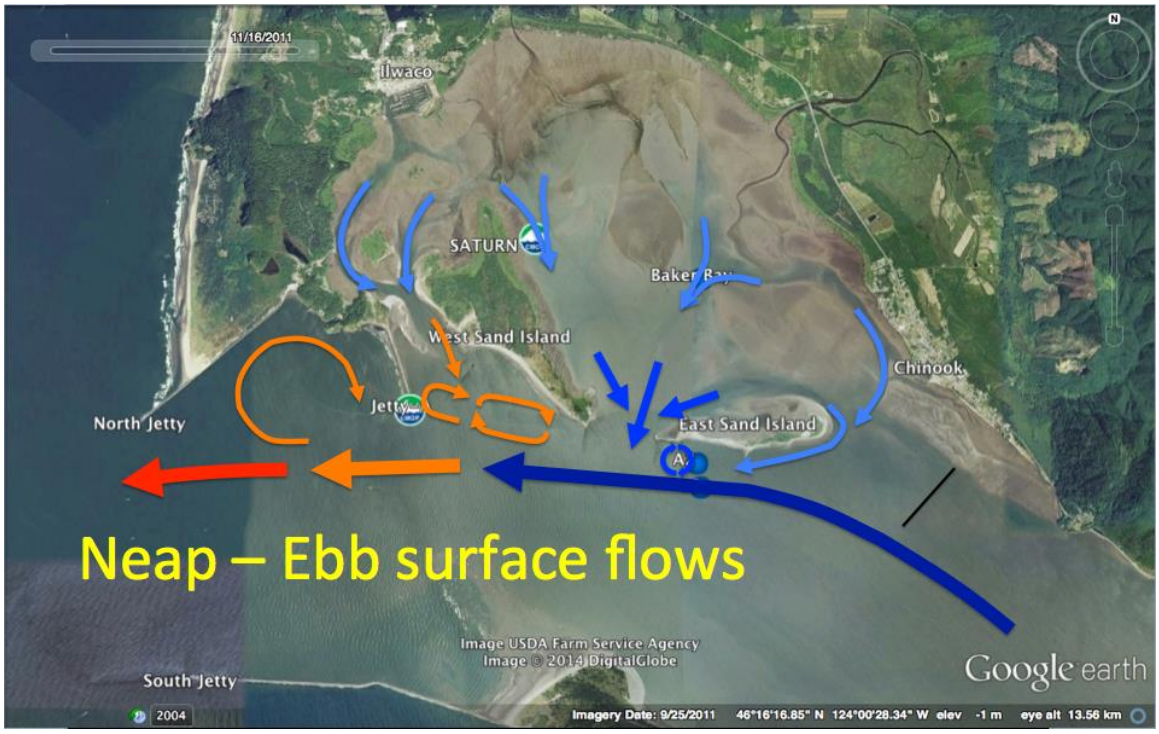

Figure 32. Simplified diagram of hypothesized surface flows during high river discharge neap tide ebb conditions. The red arrow represents ocean water, the dark blue arrow represents river water, orange arrows represent brackish (mixed) water, medium blue arrows represent cooler river-influenced Baker Bay water originating from deeper areas of the bay, and lighter blue arrows represent warmer Baker Bay water originating from shallow tidal flats. Circular arrows represent clockwise eddies formed during ebb flows.

Neap tide flood periods saw temperatures fall and salinities rise outside Baker Bay as ocean influence extended upriver (Figure 33). Temperatures at A2 and B2 dropped to 13.2°C while salinities increased to 20.2 psu during the neap tide flood (Figure 28, top and middle). Inside Baker Bay, ocean-influenced water could not reach the NPS or SATURN sensors during neap tide due to the strong river discharge, resulting in relatively fresh conditions throughout neap tide. Average salinities were 4.2 psu at the NPS sensor and 4.6 psu at the SATURN sensor (Figure 27, top and middle). During neap flood conditions, colder water (~14°C) from the deeper southern part of Baker Bay was forced northward across the sensors (Figure 33). During each neap flood flow preceding higher high water, it is hypothesized that warmer Baker Bay water was pushed toward the

eastern opening near Chinook Harbor, setting up the warm pocket of water that exited the bay and swept across the A2 and B2 sensors during the subsequent ebb (Figure 32).

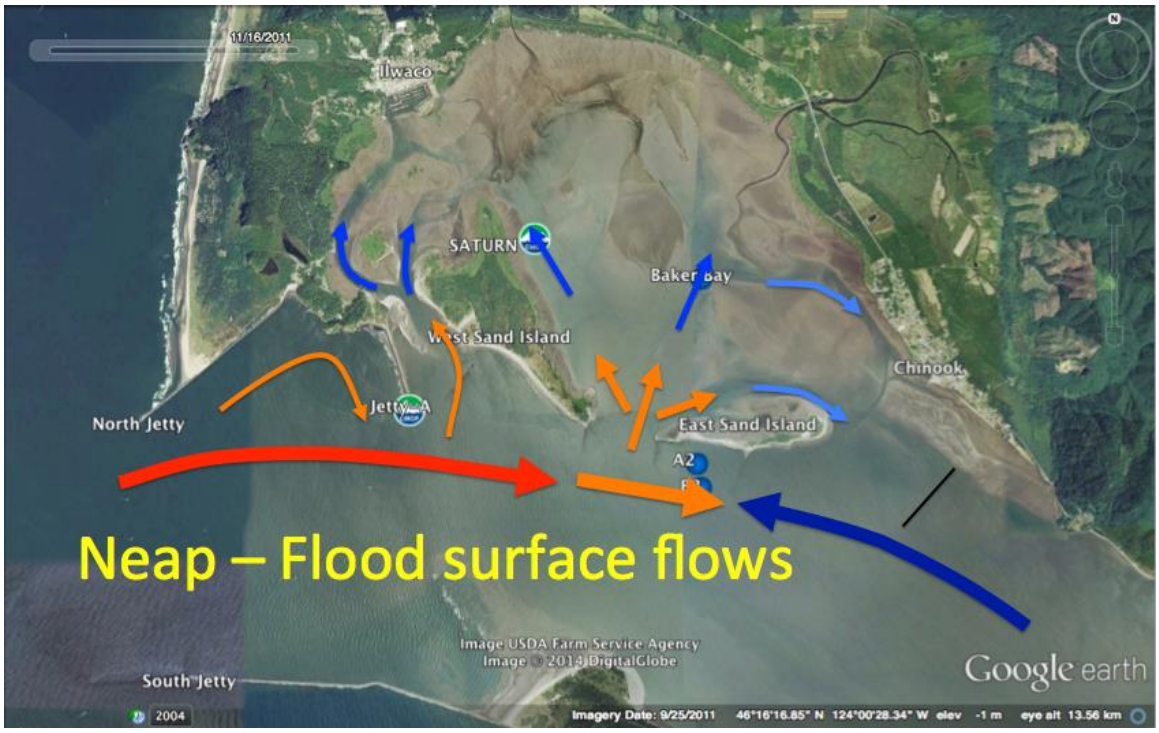

Figure 33. Simplified diagram of hypothesized surface flows during high river discharge neap tide flood conditions. The red arrow represents ocean water, the dark blue arrow represents river water, orange arrows represent brackish (mixed) water, medium blue arrows represent cooler river-influenced Baker Bay water originating from deeper areas of the bay, and lighter blue arrows represent warmer Baker Bay water originating from shallow tidal flats.

During spring tide flood periods, ocean-influenced water reached farther upriver in the main channel (Figure 34). Temperature and salinity trends at A2 followed intuitive tidal trends, with colder, higher salinity ocean-influenced brackish water evident following flood flows. Average salinity at A2 was 6.5 psu during spring tide, compared to 4.9 psu during neap tide (Figure 28, top). Spring tide water temperature and salinity trends at the A2 sensor were distinguishable from neap tide trends by the absence of temperature spikes following higher high water (Figure 28, top). It is possible that the farther-upriver incursion of ocean-influenced surface waters blocked any warm pockets

of tidal flat Baker Bay water from exiting the eastern opening of the bay (Figure 34). During spring flood conditions inside Baker Bay, cool fresh water from the deeper southern part of the bay was forced northward across the sensors (Figure 27, top and middle) while ocean-influenced water made its way farther north into Baker Bay via peripheral pathways, namely Ilwaco Channel and the eastern opening near Chinook (Figure 34).

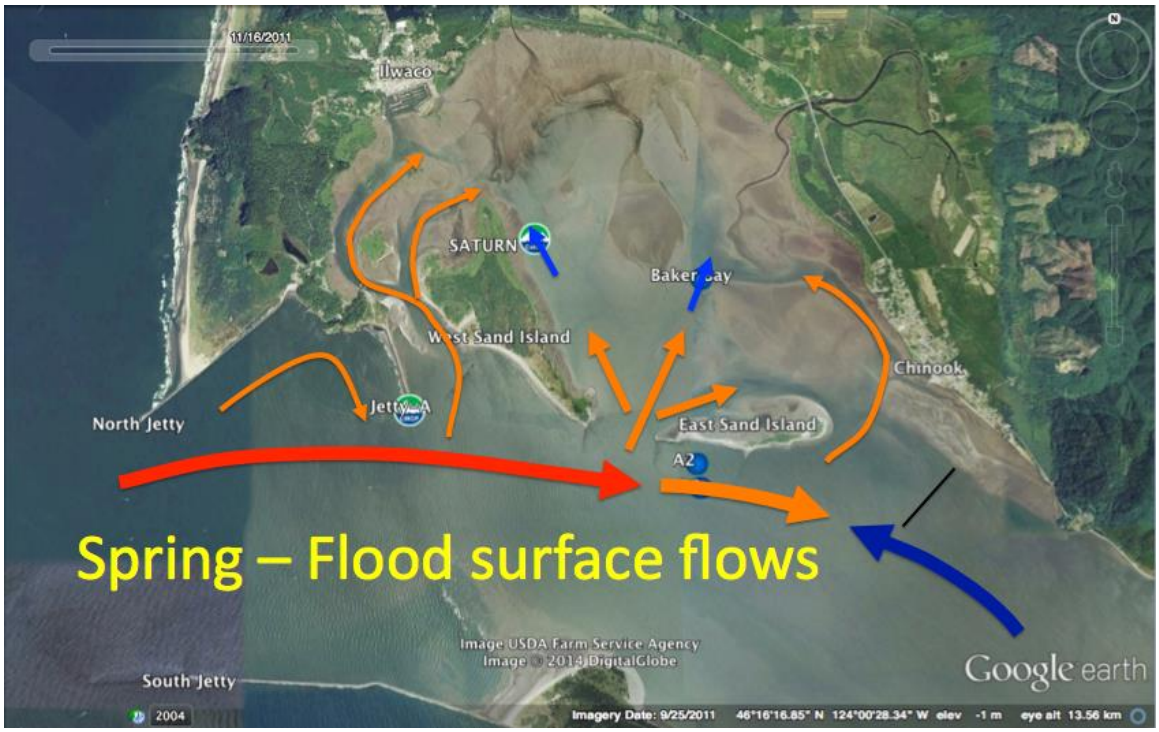

Figure 34. Simplified diagram of hypothesized surface flows during high river discharge spring tide flood conditions. The red arrow represents ocean water, the dark blue arrow represents river water, orange arrows represent brackish (mixed) water, and medium blue arrows represent cooler river-influenced Baker Bay water originating from deeper areas of the bay.

During spring tide ebb periods, downriver flows were strongest, with river-influenced fresh water evident at the A2 sensor during low tides (Figure 28 top, illustrated in Figure 35). Because river water was warmer than ocean water during this time of the year, spring ebb conditions saw temperatures rise and salinities fall in the main channel adjacent to Baker Bay (Figure 28, top). Despite the strong river discharge,

ocean-influenced water had a noticeable effect at the NPS and SATURN Baker Bay sensors during spring tide lows, especially lower low water (Figure 27, top and middle). Brackish water that had made its way far enough north along the periphery of the bay during the spring flood was now drawn southward across the Baker Bay sensors (Figure 35) toward Baker Inlet during the spring ebb. The temperature and salinity of this brackish water varied depending on the relative concentrations of contributing water masses (i.e., warm fresh tidal flat Baker Bay water, cool fresh deep Baker Bay water and cold salty ocean-influenced water). Ocean influence in Baker Bay was greater during spring tide than neap tide based on average salinities of 6.3 psu at the NPS sensor and 7.4 psu at the SATURN sensor (50–60 percent higher than during neap tide). Once again, clockwise circulations developed in the vicinity of the A2 sensor, south of West Sand Island and between Jetty-A and the North Jetty during the ebb flow.

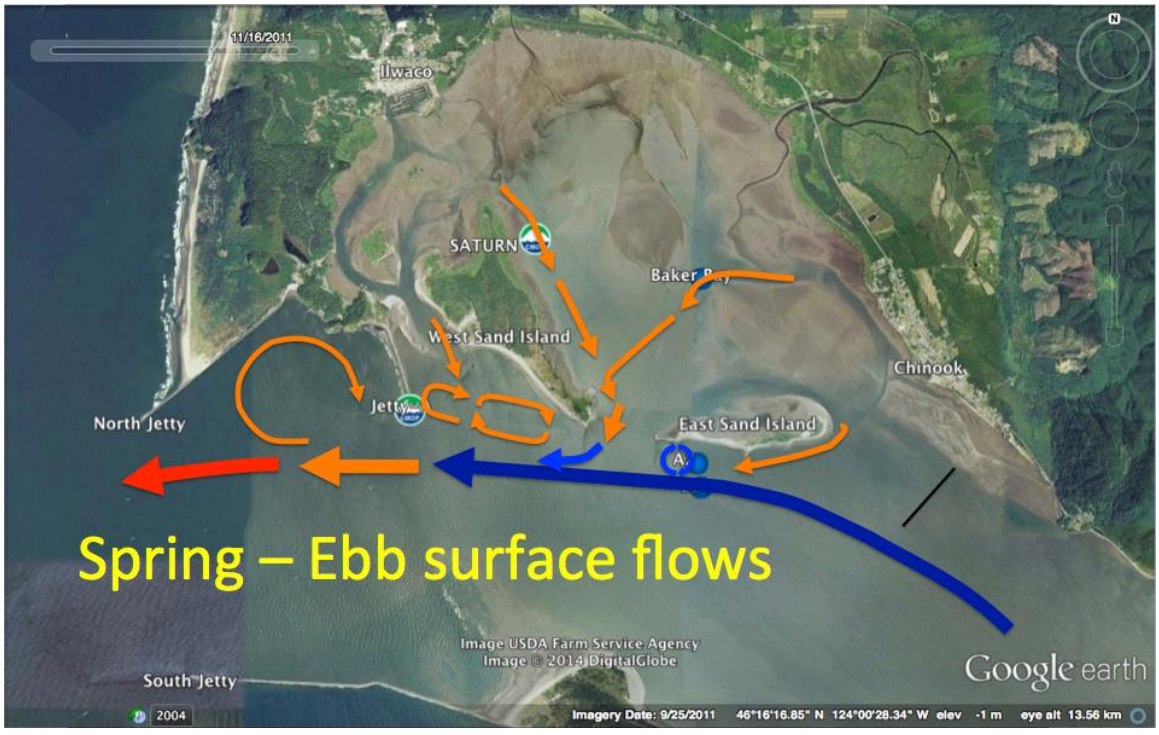

Figure 35. Simplified diagram of hypothesized surface flows during high river discharge spring tide ebb conditions. The red arrow represents ocean water, the dark blue arrow represents river water, and orange arrows represent brackish (mixed) water. Circular arrows represent clockwise eddies formed during ebb flows.

V. CONCLUSIONS AND RECOMMENDATIONS

Characterizing the flows in and around Baker Bay is challenging and depends on many factors, including the semi-diurnal tidal cycle, the neap-spring cycle, the river discharge cycle, the seasonal temperature and precipitation cycle and ocean upwelling and downwelling events. Surface winds play a role in steering surface currents, and diurnal heating plays a role in the temperature cycle of the shallow Baker Bay tidal flats.

Lagrangian surface currents show that flow is primarily confined to the main channels of the river, with some flow into Baker Bay via Baker Inlet during flood tide, especially when assisted by southwesterly winds that steer surface currents. The East Sand Island pile dikes slow down ebb flows close to the island, and shear-induced clockwise circulations form between these pile dikes east of Baker Inlet at low tides, persisting for 2–3 hours. Clockwise circulations were also observed during ebb flows west of Baker Inlet in the sheltered area between West Sand Island and Jetty-A. Flow reversals associated with these clockwise circulations were observed in the Eulerian surface velocities at A2, occurring regularly with each ebb flow. Coinciding unique slowing events related to the East Sand Island pile dikes occurred during ebb flows at B2.

Vertical velocity structure showed quasi-logarithmic profiles to varying degrees. Velocity profiles were most logarithmic in sheltered locations between pile dikes or inside Baker Bay and least logarithmic, sometimes exhibiting two-layer flow characteristics, in deeper locations experiencing more direct effects of the interactions between river discharge and tidal flow. A downriver bias in upper layer velocities was evident due to the influence of strong river discharge.

In general, the water inside Baker Bay remains fresh with transient periods of brackishness. Pure ocean water never reaches the inner parts of the bay where the two Baker Bay sensors were located. Water near the tidal flats of the northern part of Baker Bay was warmer during the data collection period due to solar insolation; this warm, fresh water was most evident during the neap tide ebb at the NPS Baker Bay sensor. Due to the location of the sensors in Baker Bay, ocean influence was indirect, as evidenced by

the observed timing of temperature and salinity changes at the sensors. Temperature and salinity shifted to a more ocean-influenced regime at low tide, not at high tide as would be expected if the pathway for ocean-influenced water were direct. It is hypothesized that small amounts of ocean water enter the bay through the western (Ilwaco) and eastern (Chinook) openings during flood conditions, mix with fresher Baker Bay water, and sweep by the sensors as cooler brackish water during ebb conditions. Water level and temperature cross-correlations at the SATURN Baker Bay sensor reinforce this indirect ocean influence concept. However, during neap tide in conjunction with higher-than-normal river discharge conditions, ocean-influenced water could not always reach the Baker Bay sensors.

Short-duration high temperature, low salinity spikes occurred south of East Sand Island during neap tide ebb flows. These warm, fresh spikes were preceded by cooler, higher salinity ocean-influenced periods at high tide. These observations suggest that during neap tide, ocean-influenced brackish water reached the A2 and B2 sensors at higher high water as flood flows into Baker Bay via Baker Inlet forced a pocket of fresher, warmer Baker Bay water out of the eastern opening of the bay. During the subsequent ebb tide, this warm pocket was carried downriver and swept across the A2 and B2 sensors south of East Sand Island. Pockets of warmer Baker Bay water were not observed at the A2 and B2 sensors during spring tide, suggesting that ocean-influenced water traveling farther upstream past East Sand Island prevented warm, fresh Baker Bay water from exiting through the eastern opening of the bay.

Further study on the water masses in and around Baker Bay is needed to better understand the hydrodynamic processes taking place in this dynamic region. A broader sensor network would preferably include Ilwaco Channel and the eastern opening to Baker Bay between East Sand Island and Chinook to more easily trace water mass characteristics and flow into and out of the bay. A network of thermistor strings would facilitate tracing the shape and movement of the salt wedge. The use of X-band radar to track tidal fronts in the lower estuary has shown promise, and efforts could be expanded to include Baker Bay and its vicinity. Finally, a hydrodynamic model using updated

Baker Bay bathymetry may provide a visualization tool for improved understanding, and the findings reported herein may prove useful in model validation efforts.

THIS PAGE INTENTIONALLY LEFT BLANK

APPENDIX A. GT-31 ACCURACY TESTING

Static and kinematic tests were conducted to determine the positional accuracy of the GT-31 handheld GPS units. Three different static test configurations were conducted, each using four GT-31s. GGA and RMC sentences were collected with a sampling interval of one second. The static tests were conducted on the roof railing of Spanagel Hall on the campus of NPS in Monterey, California. The kinematic test was conducted on the NPS quad between Spanagel Hall and Root Hall.

The first static test consisted of four GT-31s adjacent to each other, lying flat on their backs. The test was conducted on 15 August 2013 from 0915–1442 Pacific Daylight Time (PDT, 5 hrs 27 min duration). Since the GT-31s were stationary during the test, indicated track speed was considered error. Maximum speed error, average speed error and speed error standard deviation were determined for each GT-31. The maximum instantaneous position jump was calculated by finding the square root of the sum of the squares of northing and easting differences for each sampling interval. A mean position was calculated for each unit, and the 2DRMS (95 percent) radius was assumed to be equivalent to position error. Positions were not post-processed, so much of the error may be attributable to GPS satellite error. Table 5 summarizes error results from the first static test.

GT-31 #	Max speed error ($m\ s^{-1}$)	Mean speed error ($m\ s^{-1}$)	Speed error standard deviation ($m\ s^{-1}$)	Max position jump (m)	2DRMS error (m)
76	0.1080	0.0257	0.0125	0.5547	9.4672
77	0.0977	0.0234	0.0110	0.2375	4.2250
78	0.1492	0.0251	0.0119	0.3698	8.6289
79	0.1543	0.0253	0.0116	0.3987	8.4806

Table 5. GT-31 static test (flat).

The second static test consisted of two GT-31s (76 and 77) lying flat on a metal plate (to limit multipath error) a short distance (about 15 cm) apart and two (78 and 79) lying flat on the wooden railing a similar distance apart. The test was conducted on 16 August 2013 from 1005–1643 PDT (6 hrs, 38 min duration). Table 6 summarizes error results from the second static test.

GT-31 #	Max speed error ($m\ s^{-1}$)	Mean speed error ($m\ s^{-1}$)	Speed error standard deviation ($m\ s^{-1}$)	Max position jump (m)	2DRMS error (m)
76	0.1080	0.0303	0.0134	0.2375	4.9297
77	0.0772	0.0306	0.0146	0.3987	4.3053
78	0.0977	0.0303	0.0144	0.2375	4.0395
79	0.0772	0.0299	0.0142	0.2375	4.5098

Table 6. GT-31 static test (metal plate).

The third static test consisted of two GT-31s (76 and 77) lying flat on their backs and two (78 and 79) lying on their sides on the wooden railing about 15 cm apart. The test was conducted on 18 August 2013 from 1027–1752 PDT (7 hrs, 25 min duration). Table 7 summarizes error results from the third static test.

GT-31 #	Max speed error ($m\ s^{-1}$)	Mean speed error ($m\ s^{-1}$)	Speed error standard deviation ($m\ s^{-1}$)	Max position jump (m)	2DRMS error (m)
76	0.0823	0.0314	0.0131	0.2375	3.6211
77	0.1080	0.0334	0.0163	0.3509	5.1673
78	0.2212	0.0468	0.0180	0.5744	10.7575
79	0.2264	0.0416	0.0164	0.3698	4.4408

Table 7. GT-31 static test (side).

The kinematic test was conducted using four GT-31s and an Ashtech Z-Xtreme differential GPS receiver mounted on a three-wheeled golf bag pushcart. The cart was pushed at varying speeds between 0 and 1 $m\ s^{-1}$ along a 30 m × 20 m rectangular path on the NPS quad between Spanagel Hall and Root Hall on 26 September 2013 from 1358–1439 PDT (41 min duration). Position and speed errors were determined from the differences between the post-processed Ashtech measurements (assumed to be true positions) and the raw GT-31 measurements. Table 8 summarizes error results from the kinematic test.

GT-31 #	Position error max (m)	Position error mean (m)	Position error standard deviation (m)	Speed error max (m s^{-1})	Speed error mean (m s^{-1})	Speed error standard deviation (m s^{-1})
76	3.7188	1.6434	0.6022	0.4183	0.0569	0.0394
77	6.4146	2.8613	1.4837	0.3720	0.0536	0.0345
78	3.9873	1.8020	0.5490	0.5058	0.0607	0.0449
79	4.8635	2.1339	0.9195	0.4286	0.0546	0.0386

Table 8. GT-31 kinematic test.

APPENDIX B. DRIFTER DEPLOYMENT GRIDDED VELOCITY VECTOR PLOTS

Gridded velocity vector plots show the average direction and speed for all drifters that passed through a given 100 m grid box during a single drifter deployment flood or ebb cycle (Figures 36–43). Grid boxes with at least 26 independent observations were deemed high confidence, and grid boxes with 15–25 independent observations were deemed medium confidence. Black vectors represent high confidence grid velocities, and gray vectors represent medium confidence grid velocities. The red vector in the center of each plot represents a velocity of 1 m s^{-1} for scaling purposes. Solid black lines mark shore boundaries and pile dikes.

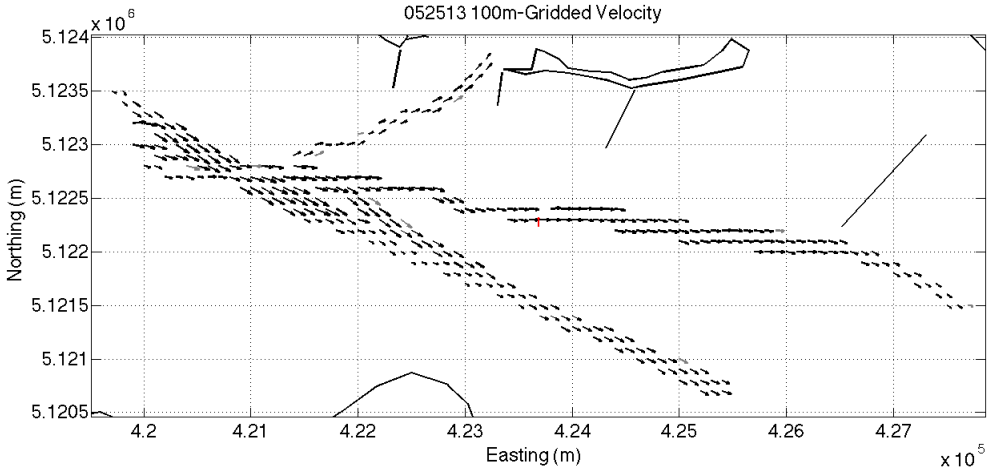

Figure 36. YD 145 gridded velocity vectors.

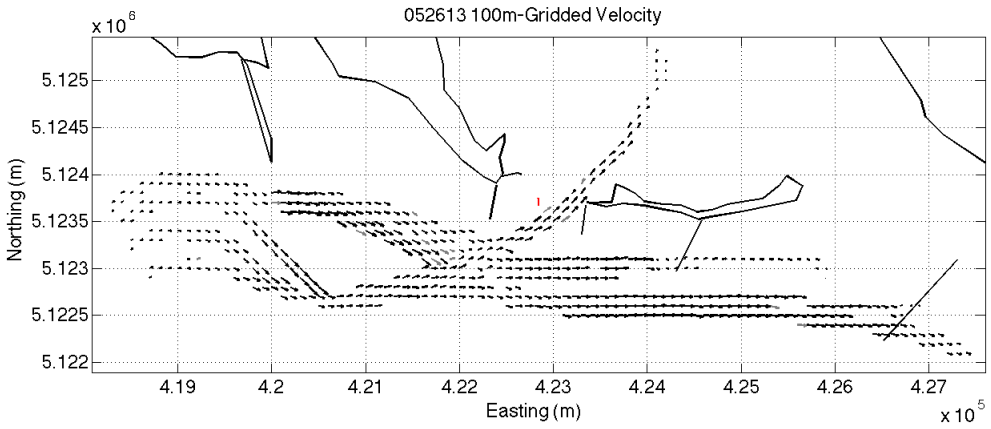

Figure 37. YD 146 gridded velocity vectors.

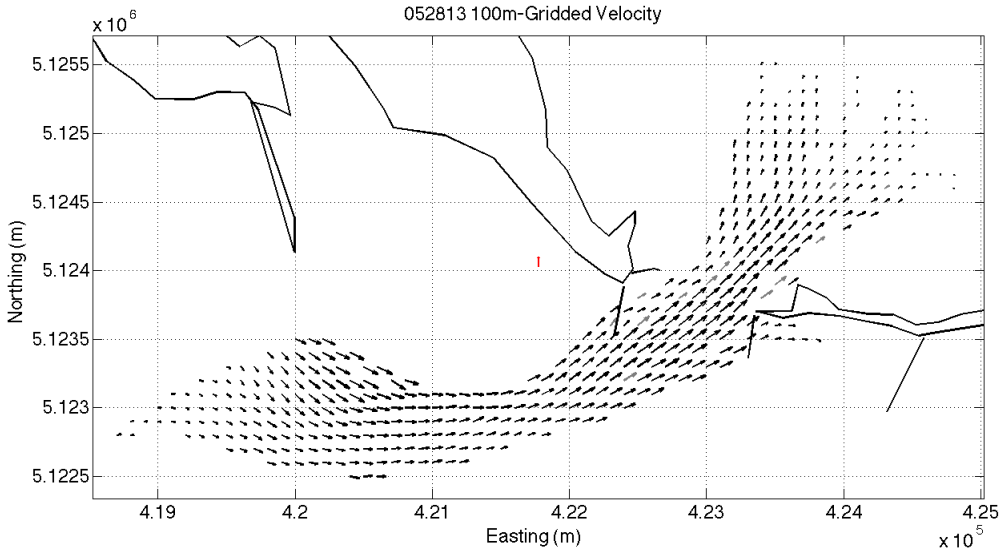

Figure 38. YD 148 gridded velocity vectors.

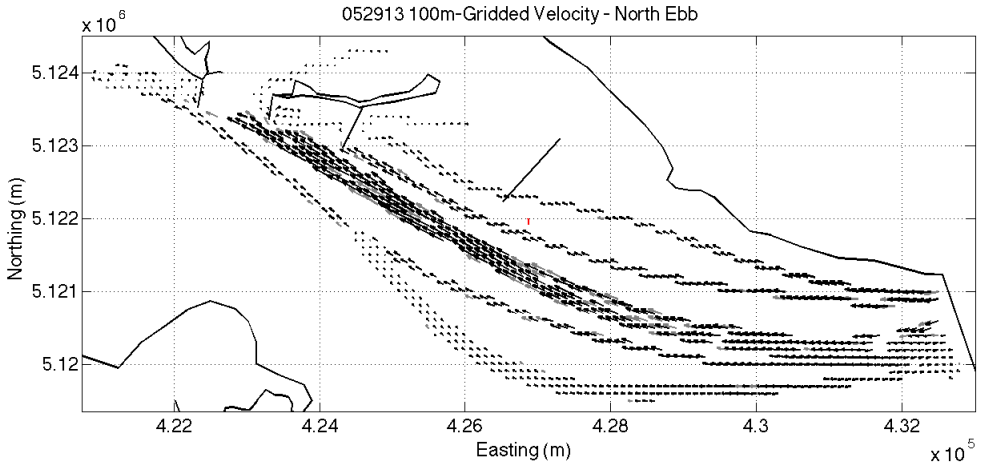

Figure 39. YD 149 north gridded ebb velocity vectors.

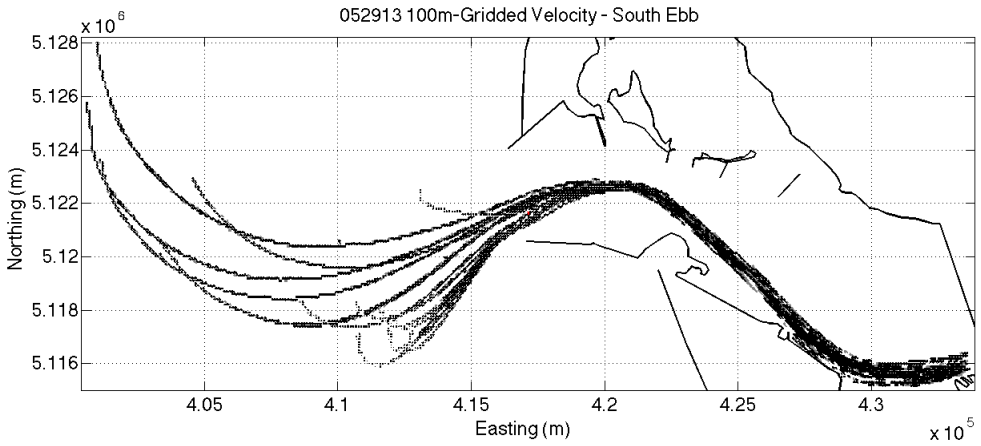

Figure 40. YD 149 south gridded ebb velocity vectors.

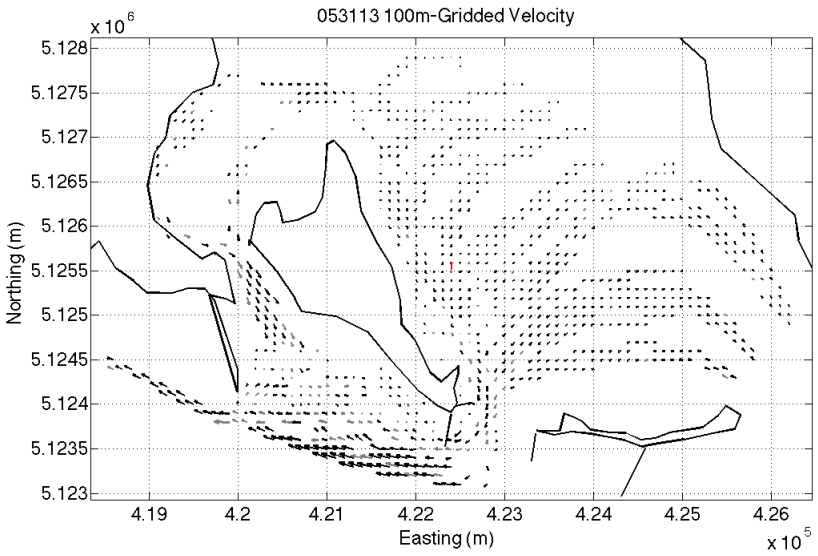

Figure 41. YD 151 gridded velocity vectors.

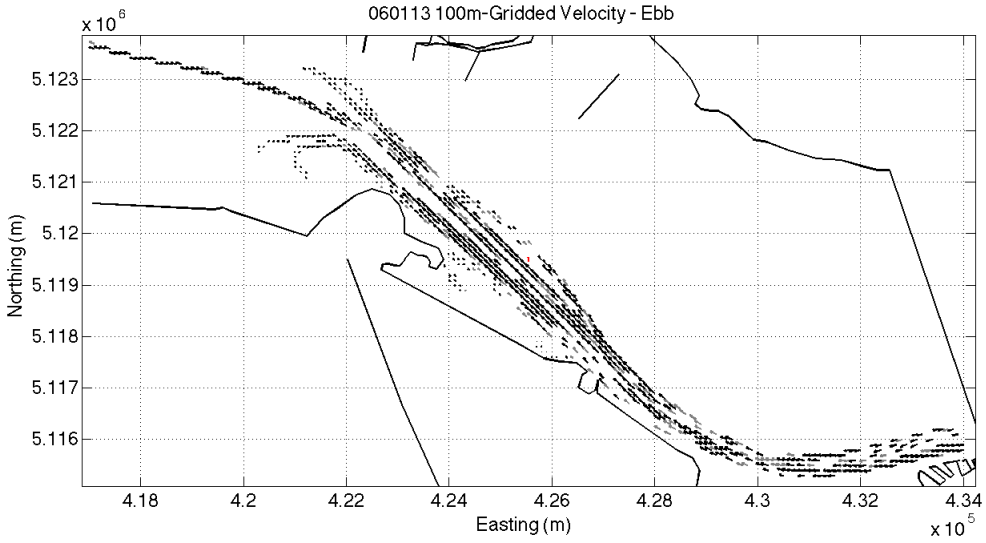

Figure 42. YD 152 ebb gridded velocity vectors.

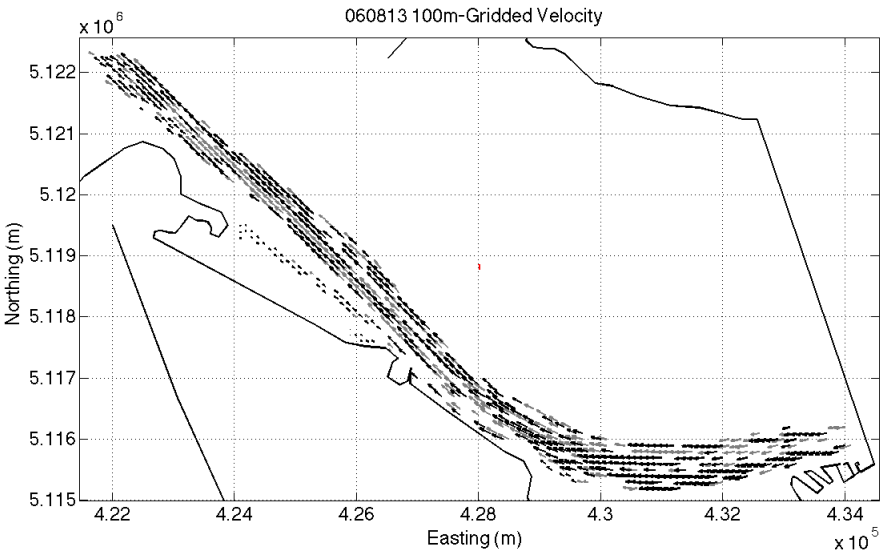

Figure 43. YD 159 gridded velocity vectors.

THIS PAGE INTENTIONALLY LEFT BLANK

LIST OF REFERENCES

AECOM, 2011: Structural and hydraulic analysis of Columbia River pile dikes. USACE Tech Rep. W9127N-10-D-0002, 90 pp.

Barnes, C. A., A. C. Duxbury, and B. A. Morse, 1972: Circulation and selected properties of the Columbia River effluent at sea. *The Columbia River Estuary and Adjacent Ocean Waters*, A. T. Pruter and D. L. Alverson, Eds., University of Washington Press. 41–80.

Bottom, D. L., C. A. Simenstad, J. Burke, A. M. Baptista, D. A. Jay, K. K. Jones, E. Casillas, and M. H. Schiewe, 2005: Salmon at river's end: The role of the estuary in the decline and recovery of Columbia River salmon, NOAA Tech. Memo., NMFS-NWFSC-68, 246 pp.

Brown, J., C. Tuggle, J. MacMahan, and A. Reniers, 2011: The use of autonomous vehicles for spatially measuring mean velocity profiles in rivers and estuaries. *Intel. Serv. Robotics*, **4**, 233–244.

Dever, E. P., M. C. Hendershott, and C. D. Winant, 1998: Statistical aspects of surface drifter observations of circulation in the Santa Barbara Channel. *J. Geophys. Res.*, **103**, 24781–24797.

Ettema, R., and M. Muste, 2004: Scale effects in flume experiments on flow around a spur dike in a flatbed channel. *J. Hydraul. Eng.*, **130**, 635–646.

Hickey, B. M., L. J. Pietrafesa, D. A. Jay, and W. C. Boicourt, 1998: The Columbia River plume study: Subtidal variability in the velocity and salinity fields. *J. Geophys. Res.*, **103**, 10339–10368.

Hickey, B. M., R. M. Kudela, J. D. Nash, K. W. Bruland, W. T. Peterson, P. MacCready, E. J. Lessard, D. A. Jay, N. S. Banas, A. M., Baptista, E. P. Dever, P. M. Kosro, L. K. Kilcher, A. R. Horner-Devine, E. D. Zaron, R. M. McCabe, J. O. Peterson, P. M. Orton, J. Pan, and M. C. Lohan, 2010: River influences on shelf ecosystems: Introduction and synthesis, *J. Geophys. Res.*, **115**, 1–26, doi:10.1029/2009JC005452.

Jay, D. A., and L. D. Smith, 1990: Circulation, density distribution and neap-spring transitions in the Columbia River Estuary. *Prog. Oceanogr.*, **25**, 81–112.

Klinkhammer, G. P., C. S. Chin, C. Wilson, M. D. Rudnicki, and C. R. German, 1997: Distributions of dissolved manganese and fluorescent dissolved organic matter in the Columbia River estuary and plume as determined by in situ measurement. *Mar. Chem.*, **56**, 1–14.

Lueck, R. G., and Y. Lu, 1997: The logarithmic layer in a tidal channel. *Cont. Shelf Res.*, **17**, 1785-1801.

Sherwood, C. R., and J. S. Creager, 1990: Sedimentary geology of the Columbia River Estuary. *Prog. Oceanogr.*, **25**, 15–79.

Uijttewaal, W. S. J., 2005: Effects of groyne layout on the flow in groyne fields: Laboratory experiments. *J. Hydraul. Eng.*, **131**, 782–791.

Wright, L. D., 1995: *Morphodynamics of Inner Continental Shelves*. CRC Press, 241 pp.

INITIAL DISTRIBUTION LIST

1. Defense Technical Information Center
   Ft. Belvoir, Virginia

2. Dudley Knox Library
   Naval Postgraduate School
   Monterey, California